Development of the Miocene Manantiales foreland basin, Principal Cordillera, San Juan, Argentina

Teresa E. Jordan Department of Geological Sciences, Cornell University, Ithaca, New York 14853-1504, U.S.A. Valerie Tamm Department of Geological Sciences, Cornell University, Ithaca, New York 14853-1504, U.S.A. 7 Walnut Street, Suite 4R, Boston, MA 02108, U.S.A. Guillermo Figueroa Universidad Nacional de San Juan, 5400, San Juan, Argentina Placer Dome Exploration Inc., Gertrudis Echeñique 30 - Piso 3, Las Condes, Santiago, Chile Department of Geological Sciences, Cornell University, Ithaca, New York 14853-1504, U.S.A. Peter B. Flemings Pennsylvania State University, Dieke Building, University Park. PA 16802, U.S.A. **David Richards** University of Arizona, Tucson, AZ 85721, Arizona, U.S.A. Ken Tabbutt The Evergreen State College, Olympia, Washington 98505, U.S.A. Terri Cheatham Department of Geological Sciences, Cornell University, Ithaca, New York 14853-1504, U.S.A.

ABSTRACT

Based on study of the ages and nature of Cenozoic nonmarine clastic strata of the Manantiales basin, at the boundary between the Principal and Frontal Cordilleras of the Andes of southern San Juan Province, Argentina, the authors interpret deformation history of the La Ramada thrust belt. The 3,600 m thick section in the Manantiales basin coarsens upward from large sandstones near the base to coarse conglomerates in the upper several hundred meters, with four smaller scale cycles of upward coarsening facies. The upper three facies cycles have lacustrine deposits at the base. In all but the uppermost cycle, the upper strata were deposited by river systems flowing subparallel to the mountain belt. The upper part of the upper cycle consists of deposits of an eastward inclined alluvial fan. Ages of the strata were determined from fission-track dating of zircons in four ash layers (17.1 to 11.5 Ma, with 2 σ uncertainties of 1.4 to 2.9 my) and magnetic polarity stratigraphy in the lower 3,000 m of the section. Thermal demagnetization revealed 18 polarity zones; these probably correlate to chrons 5n.2 through 5Er, or an age range of approximately 10.5-19 Ma for the lower 3,000 m. The authors interpret that the bases of the facies cycles, dated as 19, 15.7, 12.5, and 10.5 Ma, indicate approximate initiation ages of episodes of deformation. The authors suggest that faults in the western part of the thrust belt were active before 15.7 Ma, that principal shortening on the La Ramada fault began about 15.7 Ma, and that activity on the Espinacito thrust began about 12.5 Ma.

Key words: Manantiales basin, Nonmarine foreland basin, Magnetic polarity stratigraphy, Fission-track dates, Thrust belt history, Mlocene, Chinches Formation, Principal Cordillera, San Juan, Argentina.

RESUMEN

Desarrollo de la cuenca miocena del cordón Manantiales, Cordillera Principal, San Juan, Argentina. Se interpreta la edad de deformación de la faja plegada y fallada de La Ramada, basada en estudios de edades y facies de los estratos no marinos cenozoícos de la cuenca Manantiales, ubicada en el borde entre las Cordilleras Principal y Frontal de San Juan, Argentina. El relleno de la cuenca Manantiales consta de 3.600 metros de estratos granocrecientes, desde areniscas en la base hacia gravas en el techo. Existen cuatro subciclos de facies granocrecientes, entre los cuales

los tres superiores empiezan con depósitos lacustres en sus bases. Se interpreta que los subciclos de facies se iniciaron cuando empezaron episodios de acortamiento por los corrimientos. La edad de los estratos proviene de dataciones de 4 niveles de tobas intercaladas en la columna (por trazas de fisión en circones) que dan edades entre 17,1-11,5 Ma, con errores (2σ) de 1,4 hasta 2,9 millones de años, y de magnetoestratigrafía en los 3.000 metros inferiores de la columna. Usando un tratamiento termal de las muestras paleomagnéticas, se encontraron 18 zonas de polaridad magnética, los cuales se correlacionan con 'chrons' 5n.2 hasta 5Er cuyas edades son aproximadamente 10-19 Ma. Las bases de los subciclos de facies tienen edades de 19, 15,7, 12,5, y 10,5 Ma. El conjunto de datos sugiere un intervalo de actividad de las fallas más occidentales en la zona plegada y fallada anterior a los 15,7 Ma, un acortamiento principal de la falla La Ramada a partir de 15,7 Ma, y un acortamiento principal de la falla Espinacito a partir de 12,5 Ma.

Palabras claves: Cuenca Manantiales, Cuenca continental de antepaís, Estratigrafía de polaridad magnética, Edades de trazas de fisión,
Pístoria de una faja de corrimientos, Mioceno, Formación Chinches, Cordillera Principal, San Juan, Argentina.

INTRODUCTION

The Manantiales sedimentary basin contains sediment derived from uplift and deformation of the Principal Cordillera. Specifically, the authors hypothesize that the Manantiales basin acted as a foreland basin to the segment of the Principal Cordillera known as the La Ramada thrust belt. This paper outlines the chronologic evolution of the Manantiales basin and, in turn, of deformation in the Principal Cordillera. The authors describe major facets of the depositional environments and postulate that the facies history reflects short term episodes of deformation. In addition, the authors use these data as a partial test of the model of foreland basin response to episodic thrusting that was developed by Flemings and Jordan (1990); (Jordan and Flemings, 1990).

The Manantiales sedimentary basin is located at the boundary between the Principal and Frontal Cordilleras of the Argentine Andes Mountains, between approximately 31°45' and 32°30'S latitude (Fig. 1). The Manantiales basin is an elongate region, about 65 km in north-south length, up to 18 km wide, and with at least 3,600 m thickness of nonmarine detrital clastic strata. The western border of the basin is a reverse fault, which is the easternmost major structure of the La Ramada thrust belt of the Principal Cordi Iera (Fig. 2) (Lencinas, 1982; Alvarez and Pérez, 1993; Pérez, 1995). The eastern, or Frontal Cordillera border of the basin is a depositional contact; the basin strata and underlying Permian-Triassic Choiyoi Group (Mirré, 1966) dip at intermediate angles to the west. The largely east-verging Precordillera thrust belt lies to the east of the Frontal Cordillera (Fig 1).

The authors data include field and laboratory studies of the entire thickness of the foreland basin

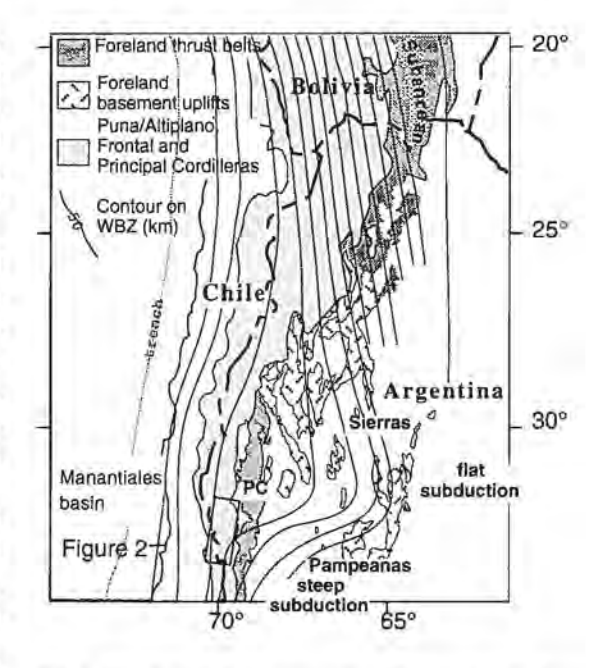


FIG. 1. The Central Andes and adjacent plate margin, from approximately 20°S to 35°S latitude. Contours on WBZ (Wadati-Benioff Zone) in km. WBZ contours define segments with flat subduction and steep subduction, with Aconcagua-La Ramada thrust belts of Principal Cordillera (see Fig. 2) spanning the transition between the segment with flat subduction and a southern segment with steep subduction. PC indicates Precordillera.

stratigraphic section. Depositional ages based on magnetic polarity stratigraphy and ash chronology, facies reconstructions, and petrographic analyses are presented and compared to the available information about kinematics and ages of structures in the thrust belt. Interpretations of the basin history shed light on the timing of major deformation in the thrust belt, specifically suggesting that three princi-

pal stages of thrusting, initiating near 19, 15.7, and 12.5 Ma, controlled deposition.

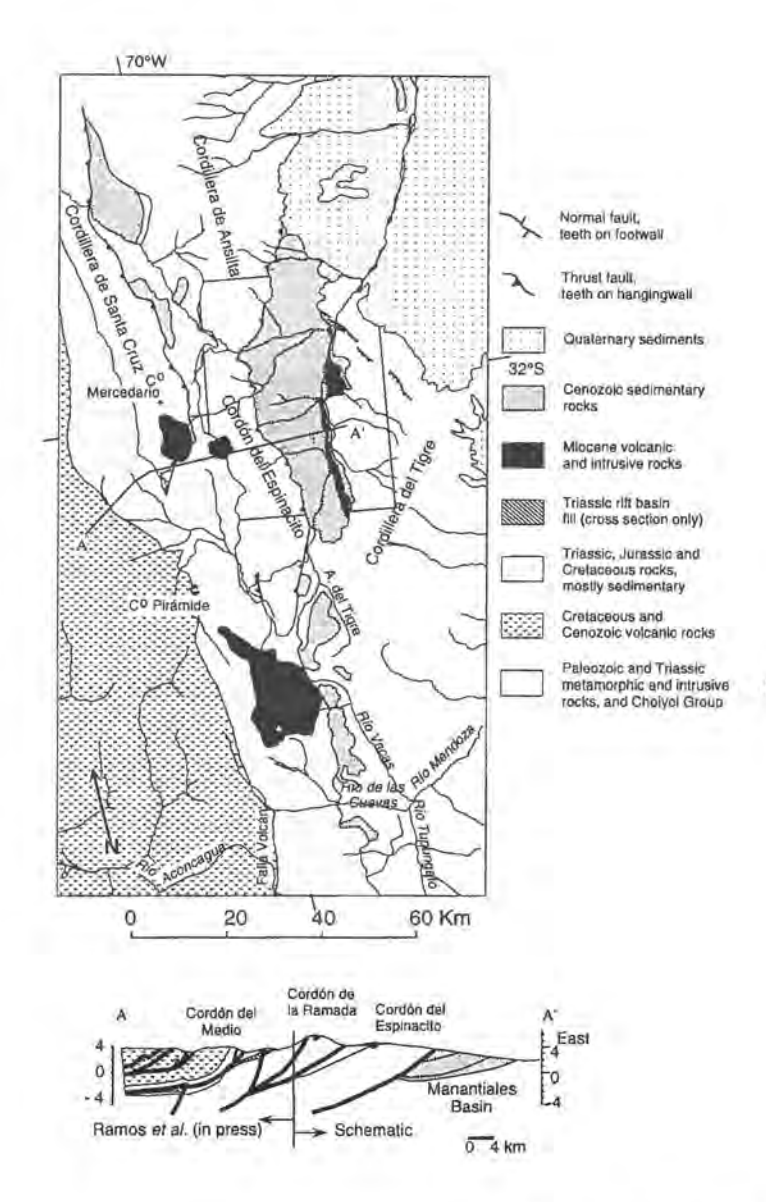


FIG. 2. Regional structure map and cross section, compiled from Lencinas, 1982; Ramos, 1985; Alvarez and Pérez, 1993; V. Ramos and E. Cristallini, personal communication, 1995a, b; Mirré, 1966; Cegarra et al., 1993; Ramos et al., 1990; Kozlowski et al. (1993) and interpretation of Thematic Mapper images. Western part of cross section is balanced (from Ramos et al., in press), whereas eastern part is highly schematic. The thrust belt in the northern two-thirds of the map area is known as the La Ramada thrust belt, whereas the southern third is the Aconcagua thrust belt. The thrust belt comprises the Principal Cordillera, whereas the Cordillera de Ansilta and Cordillera del Tigre form the Frontal Cordillera.

PREVIOUS STUDIES

STRATA OF THE MANANTIALES BASIN

Mirré (1966) referred to the strata of the Manantiales basin as the Chinches Formation. Three members were distinguished: a lower 350 m thick unit of cross-bedded sandstones and conglomerates ('areniscas chocolates'), an andesitic breccia approximately 100 m thick, and an upper clastic unit, which he estimated to be, at least 2,000 m thick ('areniscas conglomerádicas'). This paper presents a detailed study of only Mirré's upper member.

Pérez (1995) subdivided that upper member into

5 units, basec on lithologies, and reported a total thickness of approximately 1,000 m. He interpreted that an east-verging thrust fault within the basin repeats much of the section; the fault is well defined in the field south of the zone in which the authors worked (FRL, Fig. 3), but he projects it across the authors' study area. The authors argue that there is no repetition of the section they describe across such a fault. One argument against fault repetition in the authors' area of study is that neither the authors nor Perez (1995) has recognized a fault plane in well exposed rocks. Strata east of the proposed fault dip 11-17° to the west, virtually identical to strata found

west of it (11-18°), and beds can be traced with confidence across the axes of a syncline and anticline near the projected location of the fault. An equally compelling argument is that the rocks which Pérez (1995) mapped as identical units in hanging wall and footwall positions differ in remanent magnetization: his units 5 and 6 are of reversed polarity in the supposed footwall, and are dominantly of normal polarity in the hangingwall (see below). The authors speculate that the fault mapped south of the authors' study zone has less throw than what Pérez (1995) interpreted, and passes into the authors' study zone as a syncline-anticline pair.

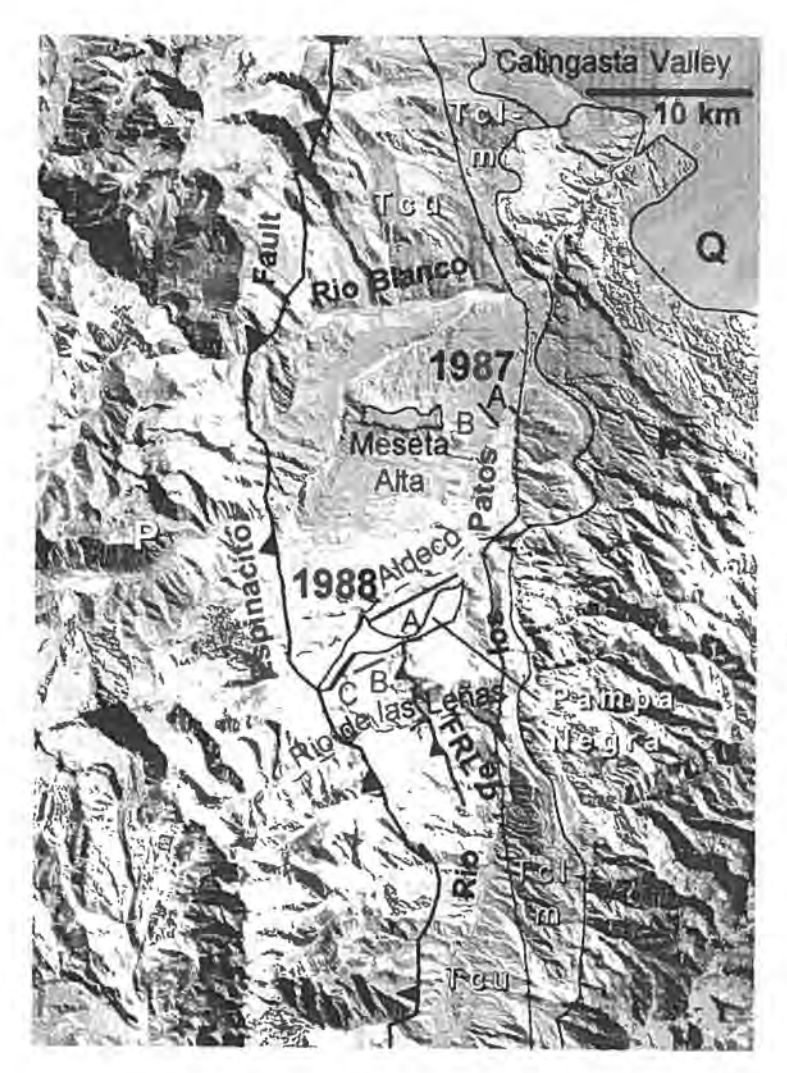


FIG. 3. Thematic mapper image and geology of center of the Manantiales basin, showing rivers, locations of 1987 ('northern') and 1988 ('southern') sections, and segments of sections (e.g., A,B,C). P= Paleozoic and Mesozoic units; Tcu= upper member Chinches Formation; Tcl-m= lower and middle members of the Chinches Formation; Q= Quaternary (?) deposits. Pampa Negra and Meseta Alta are prominent terraces on Quaternary deposits. FRL= Falla Río Leñas of Pérez's (1995). Positions of contacts based on Mirré (1966) and Pérez (1995) and image interpretation. From Thematic mapper image 232-81.

Pérez (1995) reported compositions of clasts in conglomerates throughout the section. Although it is impossible to correlate his sample locations to the authors' sections because of marked differences in stratigraphic interpretations, the authors can make general correlations between some of his map units and those described herein, based on his maps, measured sections, and comparisons of his and the authors' data sets (Pérez, personal communication, 1995). The most important of these correlations is the general equivalence of his (interpreted as repeated) unit 5 with the authors' Groups IV and VI. Pérez (1995) also reported the likelihood of a brief interval of marine influence in the basin, based on the microfossil content of one sample.

Mirré (1966) reported a Miocene age for the Chinches Formation, whereas Lencinas (1982) suggested an Oligocene age. Mirré further suggested a correlation between the Chinches Formation and the Santa María Formation, which crops out south and east of Cerro Aconcagua (Fig. 2). Ramos et al. (1990) showed that volcanic rocks intercalated near the top of the Santa María Formation are of Miocene age (8.1±0.6 Ma).

The ages of the lower two members of Mirré's Chinches Formation are not firmly established. Interpretation that the large scale cross stratification of the 'areniscas chocolates' indicates an eolian origin (Pérez, 1995) leads to tentative correlation with other Cenozoic eolian units of the region, which are bracketed between about 21 and 11 Ma (Milana et al., 1993; Jordan et al., 1993b; Yrigoyen, 1993; Sempere et al., 1994). Pérez (1995) reported that the geochemistry of the andesitic breccia that comprises the middle member of the Chinches Formation is similar to that of the latest Oligocene and early Miocene Doña Ana volcanic rocks, ca. 200 km to the north.

TECTONIC SETTING AND BEDROCK HISTORY

Today, the morphologic expression of the Manantiales basin is a north-trending broad valley at elevations between 1,900 and 3,500 m. The Río de los Patos flows northward in the valley, and converges in the northern part of the valley with the east-flowing Río Blanco (Fig. 3). The western border of the basin, the Cordón del Espinacito of the Principal Cordillera (Fig. 2), rises abruptly above the gentle slopes of the basin to average crestline elevations

above 4,500 m. Indeed, Cordón de la Ramada and Cerro Mercedario, which reach over 6,000 m elevation, lie less than 20 km west of the basin margin. In contrast, the elevation of the eastern border of the basin rises gradually to an average of 2,500 m along the crest of the Cordillera del Tigre of the Frontal Cordillera. Due to a complex definition of the boundary between the Principal and Frontal Cordilleras (Yrigoyen, 1979), the Cordillera de Ansilta, which bounds the northwestern part of the Manantiales basin, is classified as part of the Frontal Cordillera.

In the part of the Manantiales basin where the authors worked (Fig. 3), the strata are largely homoclinal, inclined to the west and northwest at 10-30°. Although the upper contact of the authors' section is a northwest-trending normal fault iAllmendinger, personal communication, 1987), most of north-trending upper contact of the basin is the Espinacito reverse fault, which is inclined 70° to the west (Pérez, 1995).

The Principal Cordillera is characterized by: abasement of Carboniferous metasedimentary rocks and Late Paleozoic and Early Mesozoic intrusive and volcanic rocks; b- a well-layered cover of marine and nonmarine strata of Jurassic and Cretaceous age, and c-volcanic and volcaniclastic rocks of Triassic, Jurassic, Cretaceous, and Cenozoic age (Fig. 2) (Yrigoyen, 1979; J.J. Zambrano, unpublished maps of San Juan and Mendoza provinces; Lencinas, 1982; Ramos, 1985a; Alvarez and Pérez, 1993). Schiller (1912); Vicente (1972) and Yrigoyen (e.g., 1979) made the pioneering studies that established the thrust style of the region, but details and regional extent of the thrust belt have been illuminated only recently through extensive mapping. Recent studies indicate that thin-skinned thrusts near Cerro Aconcagua change northward to thicker-skinned thrusts in the La Ramada zone (Ramos, 1985b; Cegarra et al., 1993; Ramos et al., 1990; Cristallini et al., 1994; Alvarez and Pérez, 1993; Ramos and Aguirre-Urreta, 1991). In both regions, the western flank of the thrust belt is constructed of Cretaceous (and/or Oligocene, according to Charrier et al., 1994) and Miocene volcanic rocks that are many thousand meters thick and which are also involved in the thrusting. The along-strike discontinuity of structural styles in the Principal Cordillera and comparatively short length of the Manantiales foreland basin probably reflects Triassic rift control on Cenozoic structural geometries. Ramos et al. (in press) and Cristallini et al. (1994) suggested that the thick-skinned geometry of

the La Ramada belt is caused by inversion of Triassic rift basins.

A major revision of knowledge of the Oligoceneearly Miocene volcanic history of the western Principal Cordillera is underway (e.g., Charrier et al., 1994), with the likelihood that much of the thick pile of volcanic rocks and volcaniclastic rocks once thought to be of Cretaceous age will be shown to be only slightly older than the Manantiales basin strata. It is presently known that arc activity was contemporaneous with the basin, as well. At the latitude of the Manantiales basin, 32°S, the Chilean flank of the Principal Corcillera exposes Farellones Formation calc-alkaline andesites and rhyolites that range in age from 19.3 to 8.4 Ma (Vergara et al., 1988); the studies of Munizaga and Vicente (1982) suggest that the majority of the volcanic rocks are older than 12 Ma. More isolated occurrences of Farellones Formation in the eastern Principal Cordillera include an andesitic complex straddling Cordón de la Ramada and Cordón del Espinacito (10 km from Manantiales basin, Fig. 2), which includes two domes whose ages are 10.7±0.7 and 12.7±0.6 Ma (Pérez, 1995).

Relatively little has been written concerning the structural style and history of the Frontal Cordillera. Its morphology, a high relief mountain range, indicates uplift above some kind of north-trending fault or fold system, but the details are poorly known. Cortés (1993) indicated that, between 32°30'S and 33°S, a high-angle reverse fault underlies the eastern flank of the Frontal Cordillera. To the north (east of the Manantiales basin), that fault system becomes non-emergent across a northwest-trending lineament (Cortés, 1993). Immediately north of the Manantiales basin, Baldis et al. (1990) and Kozlowski et al. (1993) noted that there is no conclusive evidence available of an emergent bounding reverse fault.

The Calingasta Valley (Figs. 2, 3) separates the Frontal Cordillera from the Precordillera thrust belt between 31° and 32°S. The main part of the Calingasta valley lies immediately north of, and along strike of, the Manantiales basin. Although the morphologic alignment of the los Patos and Calingasta Valleys suggests that they have a common history, available seismic profiles in the Calingasta valley reveal that there are several isolated depocenters, none of which is adjacent to the Manantiales basin (Snyder, 1988). Furthermore, the total thickness of all Triassic and Cenozoic units in the Calingasta Valley is only about 2,000 m thick in the depocenters

(Snyder, 1988), considerably thinner than the 3,600 m of Cenozoic rocks of the Manantiales basin. Therefore, there is no strong indication that the Manantiales and Calingasta basins have a direct genetic association.

Prior to completion of this study, there were few data to constrain the ages of the Manantiales basin strata and the deformation of the Cerro Aconcagua-La Ramada thrust belt. Near Cerro Aconcagua, it has been demonstrated that uplift began in the western part of the thrust belt near 21 Ma, the central thrusts had begun to deform by about 15 Ma, and deformation had progressed to the eastern margin, and ceased, by about 8 or 9 Ma (Fig. 4) (Ramos et al., 1990). Two points of information that relate to the thrust history at the latitude of the Manantiales basin both demonstrate that much of the thrusting predated about 9 to 10 Ma (Cristallini et al., 1994; Pérez, 1995).

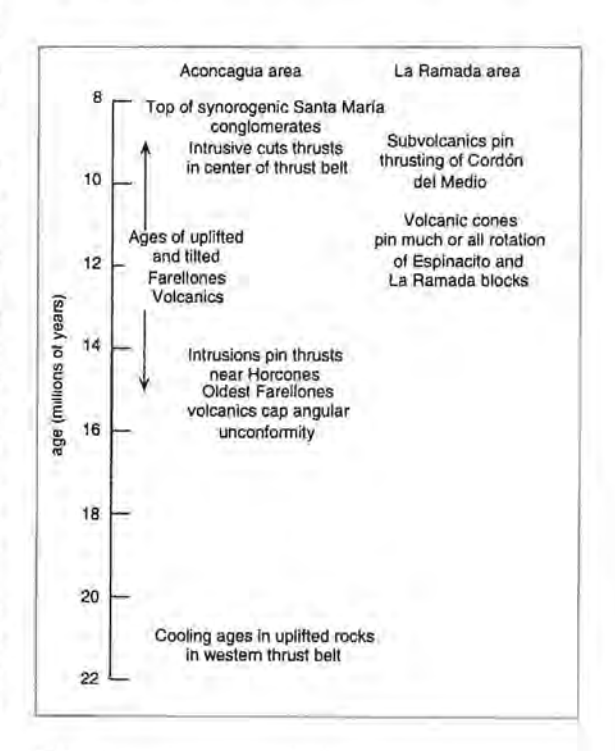


FIG. 4. Constraints on ages of deformation in Cerro Aconcagua and La Ramada thrust belts, prior to this study. Compiled from Ramos et al. (1990), Cristallini et al. (1994), and Pérez (1995).

The morphologic expression of the relict Manantiales basin is limited to the strike length of the thick-skinned La Ramada thrust belt. Elsewhere, thick-

skinned structures have generated foreland basins (e.g., Denver basin and Wind River basin in Rocky Mountains of U.S.A.). Thus, it is reasonable to hypothesize, as Pérez did (1995), that the Manantiales basin was generated by flexure beneath the La Ramada thrust load. The approximate equivalence of age of deformation near Aconcagua (21-9 Ma; Ramos et al., 1990) and age of the strata in the Manantiales basin (Miocene; Mirré, 1966) also indicates a likely genetic link. Alternatively, the Manantiales basin might be a piggyback basin formed by ponding in the syncline on the west flank of an uplifting Frontal Cordillera or Precordillera (Figs. 1. 2). To interpret the Manantiales basin as a piggyback rather than foreland basin, one would need to demonstrate that the basin filled while the east-verging Frontal Cordillera or Precordillera was uplifted. Cortés (1993) reported that strata east of the Frontal

Cordillera near 32°30'S were derived from the Principal Cordillera and, through a circuit of indirect correlations, it could be concluded that they are contemporaneous with the Manantiales basin strata, and thus that the Frontal Cordillera was uplifted after the Manantiales basin filled (Pérez, 1995). Whereas it is well documented that deformation and uplift in the Precordillera north of 31°S had begun by 19 Ma and is still active (Jordan et al., 1993a), the thrust chronology at the latitude of the Manantiales basin is not known. Thus, it is plausible that the Manantiales basin filled while it was part of the hangingwall of an active Frontal and/or Precordillera. However, the evidence presented here clearly illustrates that the La Ramada thrust system was active while the Manantiales basin strata accumulated, and thus that the Manantiales basin owes much of its existence to foreland basin behavior.

LOCATIONS AND TECHNIQUES USED IN THIS STUDY

Several approaches were used to determine the history of deformation in the La Ramada thrust belt. The most general approach is to consider the need for tectonic activity (cooling or change in crustal thickness) to produce adequate accommodation space in which a thick sediment pile can accumulate (e.g., Allen and Allen, 1990). Therefore, the mere existence of the Manantiales basin is evidence of tectonic activity; its existence next to a thrust belt strongly suggests that it is a foreland basin (Pérez, 1995). Three types of more detailed study of the strata provide clues to the histories and locations of thrust faults (Jordan et al., 1988); a- facies analysis and paleocurrent studies allow reconstruction of the depositional environments of the basin, which reflect the drainage patterns into and out of the basin. Evolution in form or style of drainage patterns indicates responses to fault activity, volcanic activity, and climate change; b- the source units of the detrital clastic sediments were determined by microscopic modal analysis of sandstones and by hand-sample identification of individual gravel clasts; if the source units are restricted to one or to a few sites in the direction indicated by paleocurrents, uplift history can be established; c- mechanical theory suggests that times of translation of thrust sheets should be times of rapid subsidence (e.g., Jordan, 1981; Beaumont, 1981; Jordan, 1995). Therefore, to the degree that accumulation rate reflects subsidence rate, an accumulation rate curve for any foreland basin sheds light on the history of deformation in the flanking thrust belt (e.g., Homewood et al., 1986; Heller et al., 1988; Flemings and Jordan, 1990).

Exposures of the strata are continuous and very good along some of the small tributaries to the Río de los Patos. Exposures are not good along the lower reaches of the major river valleys (los Patos and Río Blanco) because of cover by Quaternary terrace deposits, nor are they good at the western margin of the basin due to cover by moraines. The authors' study is based on a composite of two regions near the center of the basin (Fig. 3). The base of the section was studied east of Meseta Alta (referred to herein as the 1987 section). The most extensive continuous section studied was located in minor canyons flanking Pampa Negra, south of Arroyo Aldeco, and is referred to as the 1988 section. Correlations between the main sections and between minor segments of those main sections (Figs. 3, 18) were accomplished by field tracing of marker beds, later adjusted to be consistent with magnetic polarity zone boundaries.

Field work for this project was completed by 4 people during 7 days in January through March of

1987, and by a team of 4 during 11 days in January, 1988. The labor was focused along the vertical profile of magnetic polarity sampling sites. Facies analyses were based on rapid examination of very good exposures over a swath varying up to ca. 100

m along strike through the column. Only the most overt indicators of paleocurrent directions were measured. The authors did not make systematic observations of along-strike facies variations.

LITHOFACIES AND DEPOSITIONAL ENVIRONMENTS OF THE UPPER MEMBER OF THE CHINCHES FORMATION

The Upper Member of the Chinches Formation consists mainly of sandstones, conglomerates, mudstones and claystones. Above a conglomeratic base, the 3,600 m thick section (Fig. 5) generally coarsens upward from predominantly sandstones and mudstones in the lower third, to mostly sandstones and conglomerates in the middle, and conglomerates near the top. Three intervals of finely laminated fossil bearing claystones are also preserved; the lowest of these occurs approximately mid-way through the section.

Although there are dozens of individual lithofacies that the authors described, the strata can be broadly subdivided into eight facies groups (I-VIII, Fig. 5); each of these is defined primarily by a distinct spatial arrangement of facies and, secondarily, on the basis of predominant textures. Details of the individual facies are tabulated (Table 1). Group I was examined 5-6 km farther north than the other groups (Fig. 3). Group II was examined in both northern and southern sections. The groups are presented from oldest to youngest.

Basal 30 m. Poorly sorted sandstone with concentrations of pebbles and cobbles (≤ 20 cm diameter) comprises the basal unit, and fills erosional relief in the upper contact of the andesitic breccia member of the Chinches Formation. Bedding is weakly defined by layers of matrix supported conglomerate and lenses of clast-supported conglomerate. The clasts are entirely of volcanic and subvolcanic origin. The authors interpret this unit to represent a suite of debris flows.

GROUP I (0-250 m)

Three facies comprise Group I strata (Table 1). The first of these, light, yellowish brown, elongate, cross-stratified, multistoried conglomeratic sandstone bodies (Fig. 5, blow-up No. 1, 30-44 m and 47-50 m), accounts for the majority of sediments in the

group (ca. 80% by volume). Axes of trough cross strata trend to the east and southeast. The second one, brown to gray-green, wedge to lobate sand-stones, occurs as 3 to 5 m thick beds between successive units of the elongate sandstone and conglomerate (Fig. 5, blow-up No. 1, 44-47 m). The third facies, mudstone and sandstone sheets, occurs as a 40 m thick unit near the top of the group. Horizons of varying color are intermixed on a vertical scale of a few meters, including reds, browns and grays. Mudcracks and burrows occur locally.

Interpretations

The facies of Group I are typically fluvial deposits (Fig. 6). The elongate conglomeratic sandstones record deposition within fluvial channels, the sandstones with wedge and lobate geometries are channel-margin deposits (such as crevasse channel fills, crevasse splays, and levees), and the interbedded sandstones and mudstones, which have sheet geometries, record floodplain deposition. Two- and three-dimensional dunes migrated to the northeast and southeast down channels (Fig. 6). The paleoenvironmental significance of this will be discussed following the description and interpretation of facies from Group II.

The elongate sandstone facies may represent either single, sinuous channels or migrating sections of a large meandering river. The multiple storeys and the scarcity of overbank fines favor a meandering channel origin. Individual channels were as deep as 15 m (maximum storey thickness) and were probably hundreds of meters wide.

During flood conditions, sediment-bearing flows scoured crevasses through channel margins and deposited sandstones and mudstones onto the floodplain in lobes and sheets. Some bedform migration occurred in crevasse channels but, mostly, sands were deposited by wash-over processes, and muds

settled out of flood waters. Between these events, plants and burrowing biota inhabited the floodplain and mudcracks formed. The color variations in the channel margin sandstones and in the interbedded sandstones and mudstones probably reflect soil formation.

GROUP II (250-975 m)

Four facies comprise Group II (Table 1): a- red ribbons of cross-stratified sandstone; b- wedges,

lobes and sheets of red sandstone; **c**-red mudstone sheets (Fig. 7), and **d**- a facies with epsilon cross stratification. The first and second facies rest in contact with the third across erosional surfaces. The fourth facies is exclusive to the northern study area, and occurs adjacent to the first facies. The sandstone ribbons are typically single-storeyed, and cross-stratification within them is oriented primarily toward the northeast.

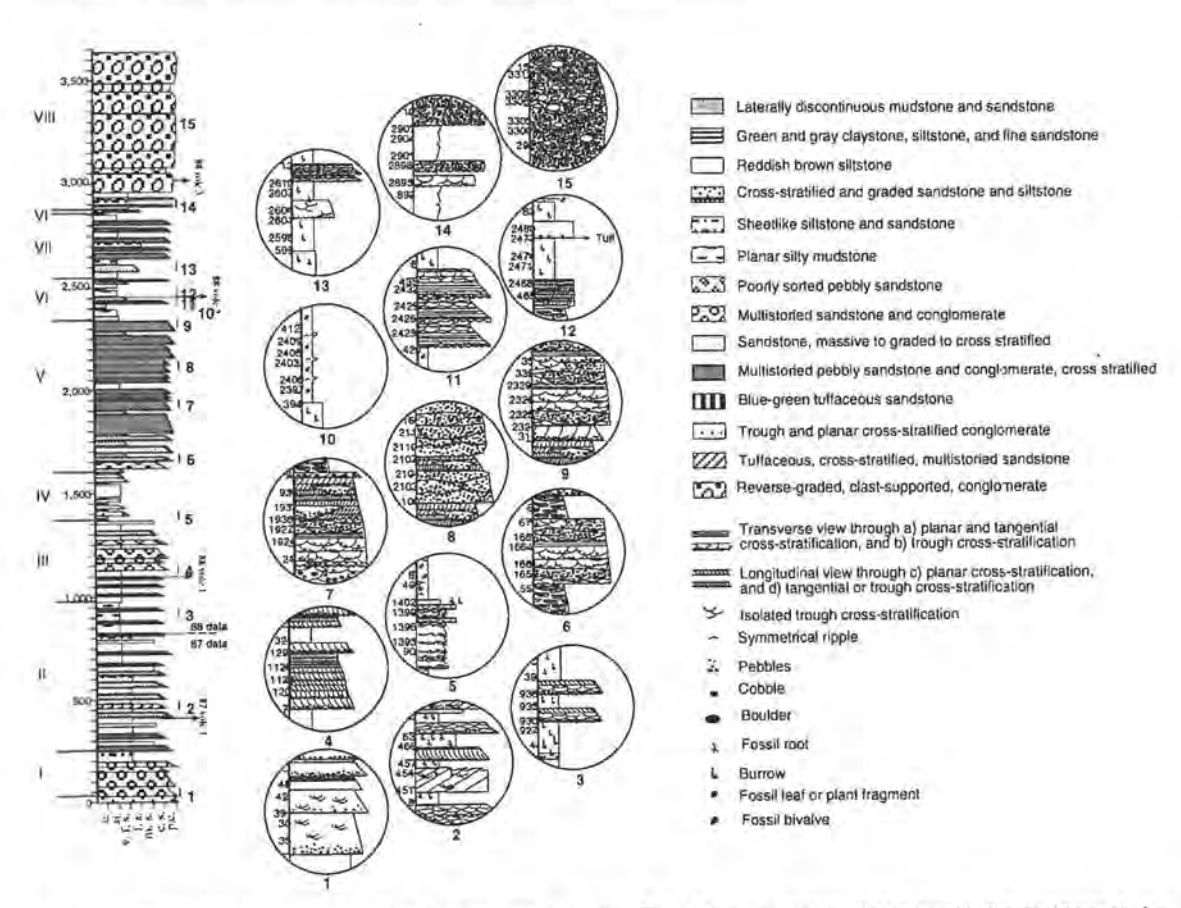


FIG. 5. Composite stratigraphic section of the Manantiales study area. The section was measured and described at decimeter scale. Some of those details are captured in the circled blow-ups to right of column; the corresponding stratigraphic levels are indicated both by the numerical scale within each circle (3 m increments), and by numbered vertical lines immediately to right of column. Roman numerals to left of column indicate facies Group subdivisions (see text).

TABLE 1. CHARACTERISTICS OF INDIVIDUAL FACIES COMPRISING FACIES GROUP I-VIII.

	Facies	Facies Dimension (Scale)	Storeys: single (s) multiple (M) thickness (m)	Basal Surface: Shape, Relief scale	Texture: fines up (f.u.); coarsens up (c.u.); grain size	Clasts: maximum particle size MPS (cm)	Sedimentary structures: type, bedset thickness	Fossil content	Other	
_	tan, elongate sandstones	5-15 m x >50 m x kilometers	S M, <5-15 m; Fig. 5 blow-up I	concave-up, 1-2 m	fining up from coarse to medium	MPS 20	trough, tangential, and planar cross stratification; -50 cr	m	dominantly tan; locally as is gray or green	
GROUP	brown to gray- green ss wedges/lobes	<3 m x 10's m x 10's m	S, <3 m	concave up or flat, cm, Fig. 5 blow-up 1, 44-48 m	f.u. from coarse to medium ss		gently dipping planar lamination; 10-15 cm	examples a	wedge-shaped djacent to elongate s; lobate examples n mudstone sheets	
S	red, brown and gray mudstone and ss.sheets	own and m x 102-103 m tlat wheets	flat	f.a. within individual laminations		lamination	1-2 mm verti mudcracks cal tubes; 2-cm-wide vertical and horizontal sandy tubes			
	red sandstone ribbons	1-12 m x 100-500 m x kilometers	S; M, 1-7 m, Fig. 5 blow-up 3	concave-up,	f.u. from coarse to medium ss	pebble clasts at base	planar and trough x-strat; 50-100 cm		narrowest rib- bons in top 70 m	
JP II	red wedges, lobes and sheets of sandstone	1-5 m x 10's m x 10's m (wedge); 1-5 m x 100's m x 100's m (lbt/sht)		concave-up or flat, cm	f.u. from medium to fine ss	some gravel lenses	some trough x-strat; <50 cm	bioturbated	thin outward from center	
GROUP	red mudstone sheets	<30 m x km2		flat				bioturbated	local cm-scale	
5	pink, inclined	1-5 m x 10's m x	M, 1-5 m	flat, inclined			tangential and trough	burrows	indivual beds	
	sandstone sheets	100's m	IVI, 1-2/III	surfaces	f.u. from very coarse to medium ss		oriented ~ 70° from elongate sandstones	inclined at 10	0°-30°; muderacks	
п	red ribbons, lenses and sheets of sandstone and conglomerate	5-10 m x 10-100 m x 100's-1000's m, Fig. 5 blow-up 4, 117-132 m	M, 5-10 m Fig. 5 blow-up 8	erosional dm		pebble clasts accentuate x-strat, MPS 3	planar (sandstone) and trough (engl) x-strat; 25-100 cm		cliff-formers; nave ribbon shape; ens or sheet shape	
GROUP III	red sandy mud- stone sheets	2-20 m x km2		flat			5-10-cm-thick sandstone beds			
10	red sandstone	~2 m x <50 m x	S, ~ 2m	concave- up	poorly sorted.		poorly-defined		vertical intervals	
GR	ribbons	100's-1000's m		or flat, cm	medium and coarse sand, and gravel		trough x-strat 5-15 m;		between units horizontal distance ntervals decrease up	
	green-yellow sandstone sheet or lens (?)	1-6 m x 100's m x 100's m		flat to slightly concave-up, cm	f.u. from medium to fine ss	poorly-sorted clasts				
	red siltstone lenses and shee	2-10 m x 10's m sx 10's m (?)		concave-up or flat, cm					mud-cracks; ween units of the ne and engl. facies	

	Facies	Facies Dimension Scale	Storeys: single (s) multiple (M) thickness (m)		Texture: fines up (f.u.); coarsens up (c.u.); grain size	Clasts: maximum particle size MPS (cm)	Sedimentary structures: type, bedset thickness	Fossil content	Other
	green claystone sheets	1,5-10 m x km2; minimum area; 14 km x 4 km	Fig. 5 blow-up 5, -1402-1411 m	flat (at least over distances of 100's of m)	fine clays with 5-10 cm-thick fine, yel- low sandstone beds		clst: finely laminated; ss: symmetrical ripples	leaves; other plant fragments	six individual horizons of this facies
P IV	yellow mudstone and sandstone sheets	6-18 m x km2 Fig. 5 blow-up 5, 1387-1401 m		flat (at least over distances of 100's of m)	f.u.		planar and trough x-strat; 0.1-0.5 m (in sandier sects.)		always overlies either the clst facies, or the ss facies
GROUP	yellow x-strat- ified sandsione (geometry?)	1-3 m x 10's-100's m x ?	S		f.u.: fine sand, gravel clasts	clasts accentuate x-strat	trough x-strat (near bases); small scale x-strat at top		typically overlie sandstone/mud- stone facies
G	red sandy mudstone sheets	<25 m x km2		flat (at least over distances of 100's of m)			10-30-cm-thick fine sandstone interbeds	The state of the s	most ss interbeds have sheet some concave up out beyond ~ 6 m
	red conglomerate sheets	0.2-2 m x 100's m x 100's m					some trough x-strat; 50-100 cm		
	red-brown mud st. sheets with encased	mudstone: dm x 10's m x 100's-1000's m		apparently flat	f.u. from sandy to silty lithologies		1		some sheets have up to 60% sand; others all silt
10	ss ribbons; Fig. 5 blow-up 6, 1652-1656 m	sandstone: -0.5 m x ~ 2 m x 100's-1000's m	S	concave-up	f.u. from medium sa with a few peb- bles to fine ss	clasts at base of sandstones; MPS -3 cm	planar cross- stratification	betw	vertical interval een units (2-10 m) decreases up
GROUP	ets with enca-	sandstone sheets; 0.2-2 m x <50 m x 100's-1000's m	Fig. 5, blow-up 6, 1657-1671 m	apparently flat	f.u.	clasts accent- uate the trough x-strat	planar x-strat; 0.1- 0.75 m; trough x-strat; 0.2-2 m	the parties	vertical interval n its encased units 0 m) decreases up
GR	sed sandstone and conglomera ribbons	ss and engl: 16 m x 10-30 m x 100's-1000's m	S	up to I m	f.u. upsection to clast size 2-	MPS increases 30 cm; average 4 cm.			frequently trun- cate one another laterally
	red-brown conglomerate ribbons	3 m x 10-50 m x 100's-1000's m	S, Fig. 5 blow-up 8, 2108-2120 m	concave-up, or flat	gravel-filled	MPS 15; average clast 3-5 cm			laterally and ly stacked with no vening sandstones
	red-brown sandstone and engl ribbons	1-12 m x 100's m x kilometers	S	erosive, but not necessarily concave-up	f.u., from gravel to medium-grained ss	MPS ~ 50	trough x-strat thins from 2.5 m at base to ~ 0.5 m at top	fossil tree roots	occurs at 7 horiz- ons and underlies all 3 other facies

table 1 continued

	Facies	Facies Dimension (Scale)	Storeys: single (s) multiple (M) thickness (m)	Basal Surface: Shape, Relief scale	Texture: fines up (f.u.); coarsens up (c.u.); grain size	Clasts: maximum particle size MPS (cm)	Sedimentary structures: type, bedset thickness (cm)	Fossil content	Other
GROUP VI	green-gray claystone and siltstone sheets			flat	of clst c.u. to cm-thick units of sits		clst: finely laminated; ss: symmetrical ripples	leaves; plant fragsments; 10-cm-thick coquina of bivalve shells	
	yellow ss and conglo- merate sheets	~16 m x 100's- 1000's m x km	M, <5-10	flat to slightly concave-up, 2 m	f.u. from gravel to medium-grained ss		trough x-strat, (especially at tops of dm to m thick	f storeys);	immediately overlies the first claystone unit
	brown mudstone sheets	~25 m x 100's- 1000's m x 100's 1000's m		flat	mudstone, with 5-20 cm thick ss inter- beds near base; f.u.		laminated	bioturbated	color varies, on -1 m scale, from brown to green
	red-brown san		sed in red-brown	mudstone sheets	(same as facies describ	ed in Group V)			
	multi-colored sandstone	~5 m x ? x ?	S	flat	well sorted fine ss		faint stratification	fragments; in	multicolored; tuff mediately overlies
	red-brown ss sheets	sheet: 1-7 m x (10's-100's m)2		- 47			trough x-strat; -20 cm		tuff horizon
M	with encased gravel and ss ribbons	ribbons: 1-1.5 m x ~20 m x 10's-100's m		some are con- cave up, some are flat					above 2100 m level, no inter- vening sheet ss
GROUP	red-brown mudstone and ss sheets	<20 m x (100's-1000's m)2					mudstone beds - 10 cm thick	em-thick fi	includes 10-40- ne-grained green sandstone layers
G	red-brown mudstone sheets	5-20 m x (100's-1000's m)2					mudstone beds ~ 10 cm thick		includes clay
1	red-brown sandy mud- stone sheets				poor sorting; c.u. from slts to fine ss, within individual	sheets	2-10 cm thick beds		facies occupies lowermost 70 m of group
UP VIII	red-brown conglomerate ribbons	-2 m x -5 m x 10's-100's m	sharp, concave- up surfaces		some trough cross stratification			cuts the sandy mude facies, and occurs at in- vertical and horizontal inte	
GROUP	red-brown ribbons and sheets of conglomerate	ribbon: 5 m x 10 m x 102-103 m sheet: <5 m x (100's-1000's m)2		mostly flat, some are con- cave up	c.u., overall; individual sheets f.u.	MPS 135; typically – dm	trough x-strat; 0.25-0.50 m; planar beds, planar lamination	F	total exposure of this facies er 450 m generally pove, generally f.u.

ss = sandstone; cngl = conglomerate; slts = siltstone; clst = claystone; x-strat = cross stratification; MPS = maximum particle size (maximum diameter)

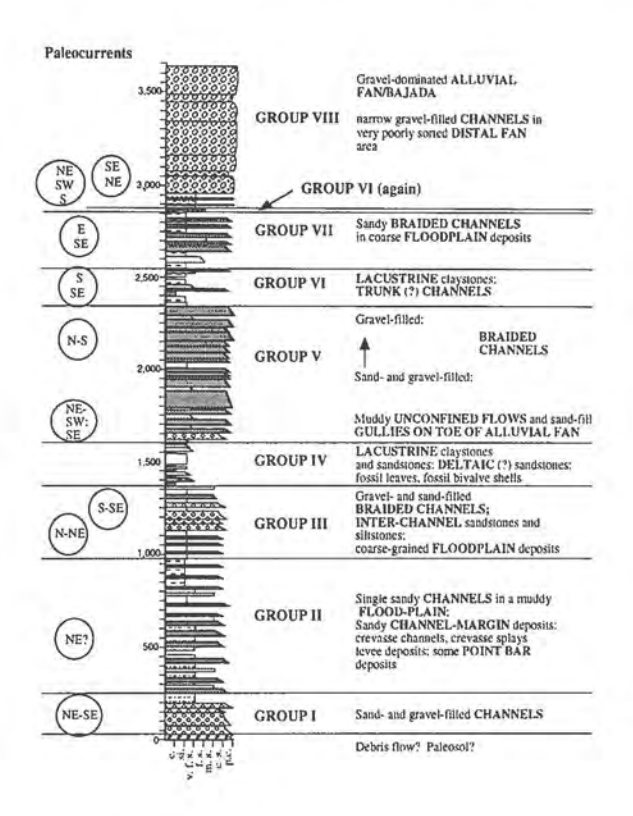


FIG. 6. Stratigraphic section with facies Groups I-VIII, interpretations of corresponding depositional environments, and summaries of paleocurrent data (in circles, to left of column).



FIG. 7. Photo of Group II facies at base of 1988 section, comprised primarily of red mudstone sheets (covered slopes) and red sandstone ribbons (resistant beds). View to northwest. Scale bar approximately 3 m stratigraphic thickness.

Group I differs from Group II in that the coarse facies of Group I are multistoreyed, with only one occurrence of an interbedded fine-grained facies, whereas in Group II coarse- and fine-grained facies alternate with one another, in units of approximately equal thickness. In addition, Group I facies have a higher sandstone to mudstone ratio than Group II facies do, and units of the elongate conglomeratic sandstone facies (Group I) are thicker than those of the ribbon sandstone facies in Group II.

Interpretations (Fig. 8)

Group II strata are also of fluvial origin. Because the sandstone ribbons are single storeyed and are sharply bounded by fine mudstone units, the authors interpret the stream style as single, sinuous channels. Despite local epsilon cross-stratification in the northern study area, and despite local multiple storeys, it is interpreted that channels changed their position mainly by avulsion rather than by migration. Individual channels were probably between 100 and 500 m wide, and 1 to 7 m deep. Cross stratification orientations, both in the southern and northern study

areas, suggest these rivers flowed primarily toward the northeast.

Overbank deposition resulted in levee deposits (wedge-shaped sandstones adjacent to elongate sandstones), crevasse channels and splays (concave-upward surfaces overlain by pebbles and cross-stratified sandstones), and sandy flood sheets (sandstone sheets). Fine muds settled from stagnated flood waters. Between flood events, floodplains were inhabited by vegetation and burrowing biota. Pedogenesis is indicated by dark brown horizons, which are probable loci of organic accumulation, and green horizons, which may be gleyed horizons where drainage was poor.

The authors suggest that the environments expressed in Groups I and II coexisted, because Group II prograded across Group I across a transitional contact. They interpret that the south and southeast flowing belt of large meandering channels of Group I was the basin axis facies, and that the sinuous rivers of Group II were tributaries from the west (Fig. 8).

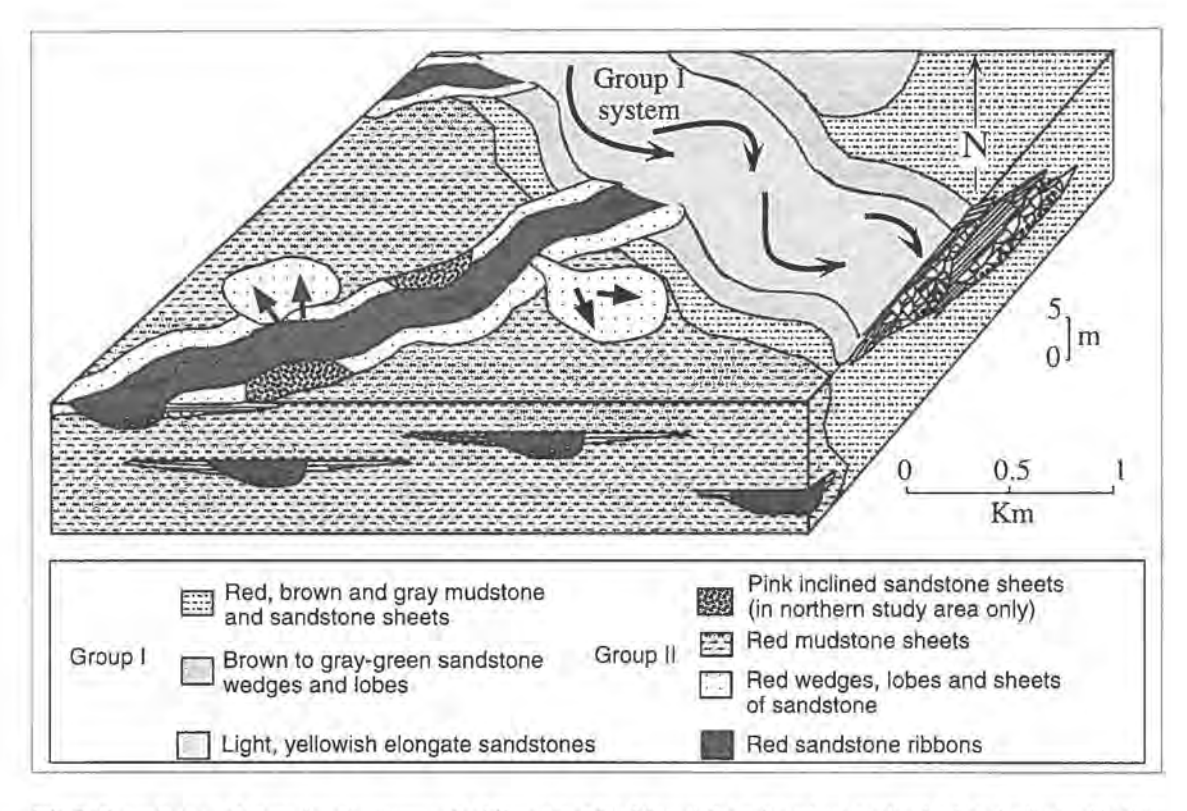


FIG. 8. Block diagram of depositional environments of Groups I and II. Although the authors have no direct data indicating that the two Groups were contemporaneous, the Group II stream channels and associated floodplains are thought to have fed a larger river system, represented by Group I facies.

GROUP III (975-1,370 m)

Five lithofacies comprise Group III (see Table 1): a- cliff-forming stacks of ribbon, lens and sheet shaped cross stratified red sandstones and conglomerates (Fig. 5, blow-up No. 4); b- red sandy mudstone sheets; c- poorly sorted, cross stratified red sandstone ribbons; d- green-yellow sandstones whose geometry, either sheet or lens, is uncertain, and e- lenses and sheets of red siltstone. The cliff-forming ribbons (lithofacies 1) are 10-100 m wide, 5-10 m thick, and estimated to be kilometers long; the cross stratified ribbons (lithofacies 3) are narrower (<50 m wide), thinner, (ca. 2 m thick), and 100's to 1,000's of meters long. The lowest 150 m

and the uppermost 60 m of Group III are comprised of the sandy mudstone sheets (lithofacies 2) crosscut by the thin, poorly sorted, ribbon-shaped sandstones (lithofacies 3) and the green-yellow sandstones (lithofacies 4) (Fig. 9, lower part); the lateral and vertical distance between successive sandstone horizons decreases upward. The middle interval of Group III strata consists primarily of the cliff-forming stacked sandstone and conglomerate facies (Fig. 9, above bentonite); siltstone units occur as lenses and sheets between stacks. Cross-stratification in the stacked sandstone and conglomerate facies is oriented to the south-southeast and to the north-northeast.

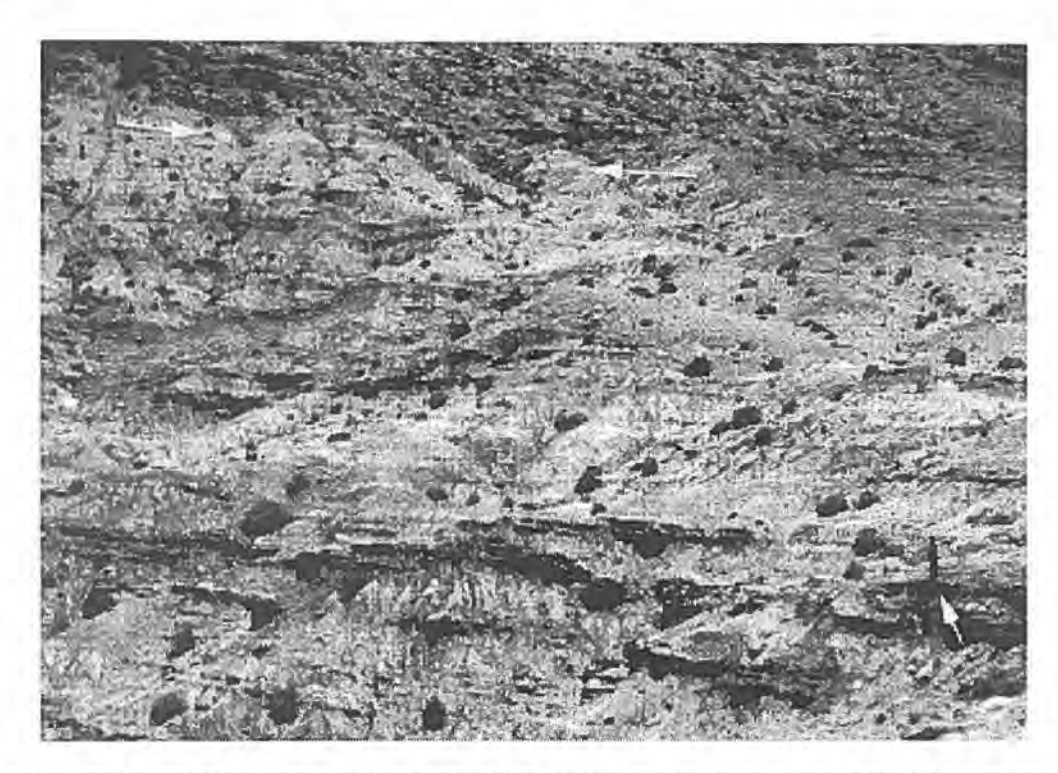


FIG. 9. Photo of lower part of Group III. Below the bentonite bed (indicated by white arrows; 88 voic 1 of Fig. 5) sandy mudstone sheets are cross-cut by thin, poorly sorted, ribbon-shaped sandstones and green-yellow sandstone sheets. Above bentonite horizon begins a thick interval of cliff-forming stacked sandstone and conglomerate facies. Person (note arrow) for scale.

Group III lithofacies differ from Group II as follows: a- the finest-grained facies of Group III (sandy mudstone) is coarser than that of Group II (mudstone), and b- Group II lacks the cliff-forming stacked sandstones and conglomerates.

Interpretations (Fig. 10)

The lower 150 m of Group III record progradation.

This interpretation stems from 1) the change from a muddy floodplain facies in Group II to a sandier one in Group III, and 2) the upward decrease in spacing (both lateral and vertical) between successive units of the green-yellow sandstone facies and the red ribbon facies (Fig. 10: bottom half of block diagram). The upward decrease in sandstone spacing may

also result from a decrease in depositional rate from Group II time to Group III time (see below). The 5-10 cm thick sandy mudstone sheets record deposition in flooded areas between narrow channels.

As progradation continued, the channels enlarged, evolved to braided morphologies, and transported sandstones and gravels from a western highland source (Fig. 10: top half of block diagram). Wide variation in paleocurrent orientations is con-

sistent with a braided channel interpretation. The channels, hundreds of meters wide and at least 5-10 m deep, accumulated gravel and sandstone ribbons in their deepest reaches. Lens and sheet-shaped deposits record deposition on gravel and sandstone bars, and along channel margins. The upper 60 m of Group III record a period during which the thinner, narrow ribbon channels again sufficed to transport sediment eastward.

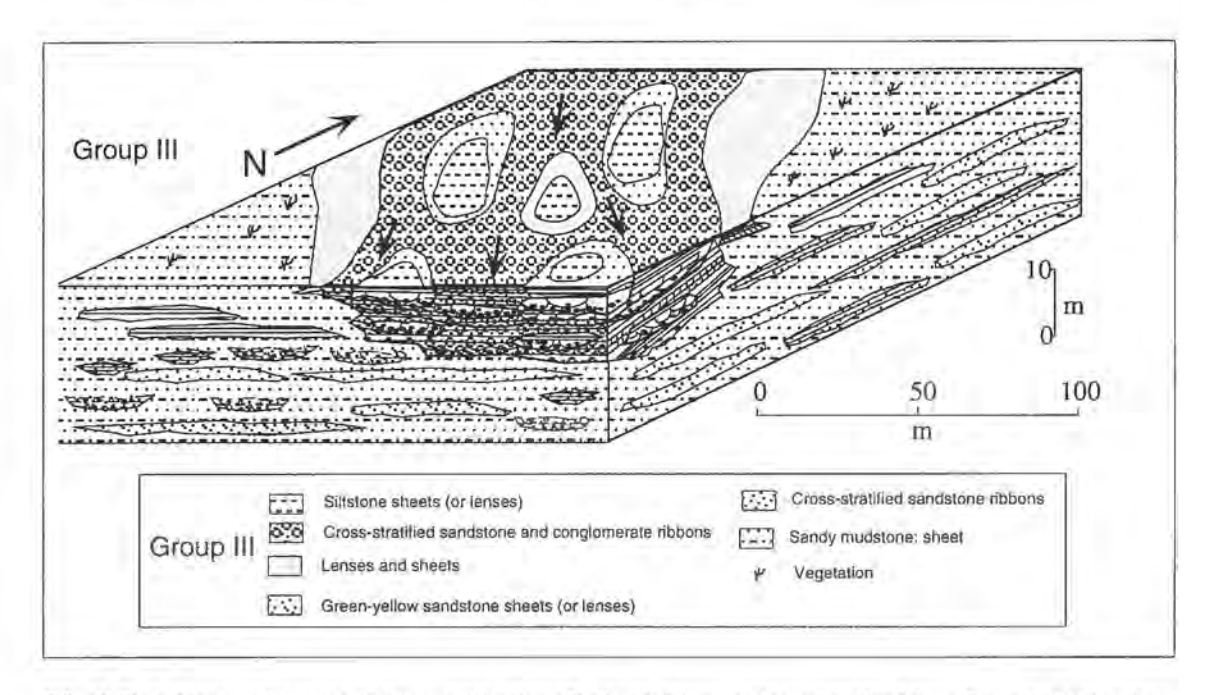


FIG. 10. Block diagram of depositional environments for Group III, a braided stream and associated floodplains. Facies designations here correspond to those described in table 1 and text. See figure 5 for additional explanation of symbols.

The authors interpret that the fundamental drainage pattern of Group III time was similar to that of Group I and II time: a western source, an east-dipping alluvial plain, and an eastern valley axis with flow roughly south-southeast. However, the distance between the source area and the study area apparently was less during Group III time than it was during Group I and II times, and thus the depositional gradient was greater and the facies differed.

GROUP IV (1,370-1,600 m)

This group consists of six intervals of finelylaminated green claystone that typically are overlain by a facies of yellow mudstone and sandstone sheets that is overlain, in turn, by a yellow crossstratified sandstone facies (of uncertain geometry) with cross-stratification accentuated by gravel clasts (Fig. 5, blow-up No. 5). Plant fragments are common in the green claystones. The claystone facies includes 5-10 cm thick yellow sandstone layers with symmetrical ripples; float from these alternating green and yellow horizons generates a distinctive soil which can be recognized on LANDSAT Thematic Mapper images, and traced for kilometers (Fig. 11). The claystone is always overlain either by the yellow mudstone and sandstone facies or by the yellow sandstone facies. In some horizons near the top of Group IV, a red sandy mudstone facies lies between the two yellow facies; this facies is cross-cut by a red conglomerate facies.



FIG. 11. View to the north of multiple claystone units of Group IV in 1988 section (from center of photo, ascending nose of ridge to left). On second ridge in photo, the inclined Group IV strata are overlain across an angular unconformity by Quaternary terrace deposits. In the middle plane of photo, Meseta Alta terrace deposits overlie Group IV alternating claystones and sandstones, immediately west of the 1987 section.

Interpretations (Fig. 12: lower zone)

Group IV strata record the first of three time intervals of lacustrine deposition in the Manantiales basin. Based on the aerial extent and thickness of the claystone units (Table 1), the authors estimate these lakes to have occupied an area of at least 4x14 km, and to have been tens of meters deep.

Because the yellow mudstone and sandstone facies always overlie the green claystone facies (Fig. 12), the authors believe the yellow mudstone and sandstone facies were deposited as lake deltas. The yellow cross-stratified sandstone facies accumulated in individual deltaic channels.

The upper part of Group IV strata (red sandy mudstone sheets and red conglomerate sheets) records an environment similar to that in which sediments near the base and top of Group III were deposited. In this case, however, confined flow was scarce, and sediment size was generally coarser. GROUP V (1,600-2,380 m)

Second only to sediments from the youngest group (see below), those of Group V are the coarsest

in the study area; they form an 800-meter-thick series of cliffs which readily distinguish this group from strata above and below it (Fig. 5). In the lower part of the group the dominant facies is mudstone sheets which encase sandstone ribbons (Table 1); (Fig. 5, blow-up No. 6: 1,652-1656 m); these are overlain by cross stratified sandstone sheets with encased sandstone and conglomerate ribbons (Fig. 5, blow-up No. 6: 1,656-1,670 m, blow-up No. 7). In the upper part of Group V, the dominant facies is laterally and vertically stacked conglomerate ribbons (Fig. 5, blow-up No. 8: 2,108-2,120 m) (Fig. 13). Cross stratification in the ribbons described above is dominantly oriented toward the northeast and southeast, with minor occurrences toward the southwest. The final facies in Group V is characterized by larger-scale ribbons of conglomerate and sandstone (ribbons of this facies are hundreds of meters wide, whereas all the previous ribbon facies noted in Group V are a few meters to 50 m wice) and greater along-strike continuity.

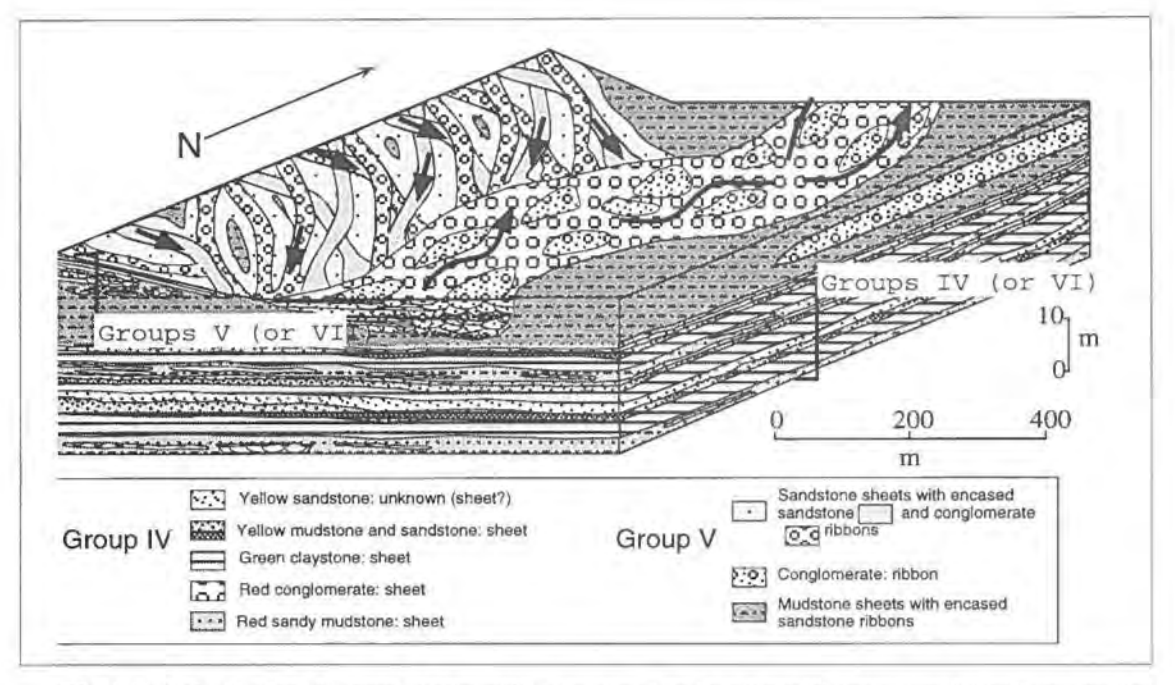


FIG. 12. Block diagram of paleogeography for Group V time, but also applicable to Group VII. Group V (and VII) facies accumulated in low-order, gravelly, transverse braided streams (eastward-inclined depositional surface on left wide of block), that is projected to have interfingered with an axial drainage system. The shallow subsurface shows the tabular distribution of lacustrine-related environments of Group IV (and also applicable to Group VI). Facies designations in Groups IV and V correspond to those described in table 1 and text.

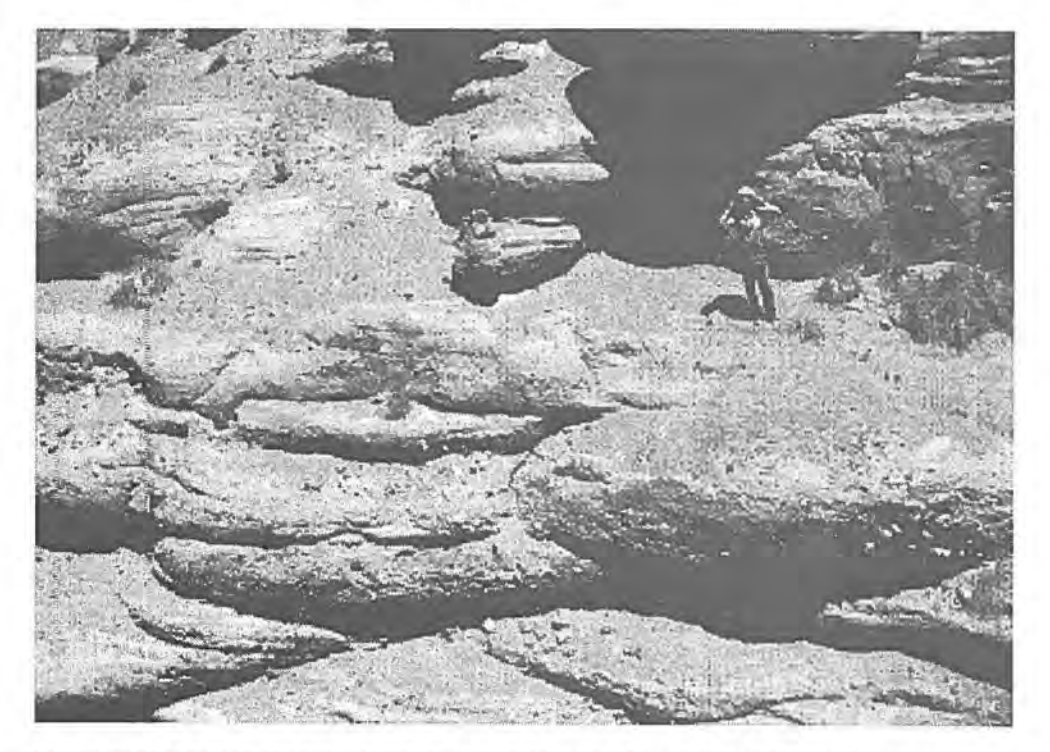


FIG. 13. Photo of stacked conglomerate ribbons in the middle part of Group V (near 2,000 m horizon).

Interpretations (Fig. 12: upper zone)

The mudstones with encased sandstone ribbons of the base of this unit suggest deposition on a distal alluvial fan: the mudstones from debris flows or sheetfloods, and the sandstones from channelized flow down gullies. Braided-stream deposition is indicated by all the other facies of this group (Table 1). Sediments transported within the northeast- and southeast-trending braided channels coarsened progressively through time and the channels widened and deepened, either as the distance between these channels and their sediment source decreased, or as discharge increased.

The wide conglomerate and sandstone facies stand out in this group, in that they record deposition in significantly larger channels. It remains unclear whether these were much higher-order streams to which the smaller braided streams were tributary (as illustrated in Fig. 12), or whether these were somewhat larger but similar in order to the majority of braided streams. If these are of much higher order, the episodic recurrence of this facies may have resulted from lateral shifts of the topographic axis, such that an extant trunk system (this facies) alternately approached and retreated from a sediment

source area that generally migrated toward the east (see below).

GROUP VI (2,380-2,560 m)

The fine-grained nature of Group VI, which bears many similarities to Group IV, contrasts markedly with the underlying Group V (Fig. 5, blow-up No. 10). In addition to a green-gray, laminated, claystone and siltstone facies containing bivalves, fossil plantfragments (Fig. 5, blow-up No. 12, top), and symmetrical ripples, four other facies are preserved (Table 1). The first facies consists of single and multiple storeyed cross stratified sandstone and conglomerate sheets (Fig. 14; Fig. 5, blow-up No. 11); cross-stratification is oriented toward the east and southeast. This facies separates and overlies two intervals of claystone and siltstone facies. Sandstones of this sandstone and conglomerate facies comprise one of the most readily recognizable and widely traceable units in the Manantiales section. Other facies in Group VI include mudstone sheets, sandstone ribbons encased within mudstone sheets (identical to the facies preserved in the lower sections of Group V), and narrow, multi-colored sandstone bodies that overlie tuff horizons.



FIG. 14. Photo of single and multiple storeyed cross-stratified sandstone and conglomerate sheets in Group VI, which constitute deposits of an axial channel system that alternated with lakes. View to the west. This facies forms a laterally traceable unit, and is an important tie between the authors' units and those of Pérez's (1995). Scale bar approximately 5 m stratigraphic thickness.

Interpretations

Group VI strata represent the fill of lakes (greengray claystone and siltstone facies) and deposits of a major trunk stream (single and multiple storeyed sandstone and conglomerate sheets); because these scenarios are similar to those of Group IV and the last facies of Group V, figure 12 serves again as an illustration. Two separate lakes are recorded by claystones in this group. Water depth in the older lake was somewhat greater than 30 m (maximum unit thickness) and in the younger lake was no deeper than 15 m. Wave ripples formed at times of shallower water.

Large rivers occupied the topographic axis of the basin between and after the time intervals with lakes. The multistoreyed nature (lower occurrence of sandstone and conglomerate sheet facies) and lateral extent (both occurrences of this facies) suggest that the channels meandered within several kilometers wide channel belts. Individual channels were probably, at least, 10 m deep (storey thickness) and may have been on the order of hundreds of meters wide.

The east and southeast flow of major channels implies a significant change from the northeasterly-directed trunk system proposed for Group V. The authors speculate that regional tectonic activity may have initially blocked an older northeast-flowing drainage and, eventually, redirected the drainage. In the case of the second lake deposit, however, an equally likely scenario is that deposition was triggered by volcanic activity (recorded by an interbedded volcanic tuff) which temporarily blocked drainage out of the basin.

The third and fourth facies in Group VI record deposition on the floodplain and tributaries of these meandering large channels. The origin of the multi-colored sandstone is unclear.

GROUP VII (2,560-2,840 m)

Group VII constitutes another cliff-forming sequence dominated by cross-stratified sandstone sheets with encased conglomerate and sandstone ribbons (Fig. 5, blow-up No.13, 2,610-2,614 m), a facies that is similar to, but finer than, the second facies of Group V (Fig. 15). Above the 2,660 m level, the conglomerate ribbons are laterally and vertically adjacent to each other, rather than encased in sandstone sheets. Trough cross-stratification, within both the cross-stratified sandstone sheets and the conglomerate and sandstone ribbons, is oriented toward the east and southeast. Additional facies comprise

interbedded sheets of mudstone and sandstone, and mudstone sheets (Table 1). There is a progression upward in the unit from mudstone sheets to combined mudstone and sandstone sheets.

Interpretations

Facies of Group VII strata record braided stream deposition similar to that of Group V (Fig. 12). Stacked sandstones and gravels were deposited both as braided channel-fill and as inter-channel bars, whereas the mudstone and sandstone sheets were deposited in distal areas of the braided fluvial system. The upward coarsening of both (the channel deposits and the sandstone and mudstone sheets) implies a progradation of the braidplain system. Compared to the Group V depositional system, the channels were smaller (up to 20 m wide, rather than 30-50 m wide) and accumulated finer grained sediments.

GROUP VI (2,840-2,855 m), again

Strata characteristics of Group VI are repeated between Groups VII and VIII: three thin (1-2 m thick) green claystone units, with interbedded fine-grained sandstones and 10 cm thick carbonate beds. The total unit thickness (including three distinct claystone beds, three distinct sandstone beds, and two carbonate beds) is approximately 15 m.

Interpretation

The claystones represent lacustrine deposition. The authors do not know the full aerial extent of these lakes but, considering how thin the individual claystone units are, the lakes were probably not very deep (2-3 m deep). The lakes may have been significantly smaller than those whose sediments are preserved in Group IV and in the first occurrence of Group VI.

GROUP VIII (2,855-3,632 m)

The base of the uppermost group is a facies of poorly sorted, sandy, mudstone sheets, cross-cut by a facies of conglomerate ribbons (Fig. 5, blow-up No. 14). These rocks coarsen upward to stacks of another facies, one of laterally and vertically juxtaposed sheets and ribbons of cross-stratified conglomerate (Fig. 16). Individual conglomerate sheets commonly fine upward and are characterized by planar bedding and planar lamination (Table 1) (similar to the alluvial-fan sheetflood 'couplet' facies described by Blair and McPherson (1994, p. 470); lateral continuity of these beds is on the order of tens of meters. Conglomerate ribbons are less common; trough cross-stratification sets within them are oriented toward the northeast, southeast, south, and

southwest (Fig. 6). Oversized clasts are common. From the base of Group VIII to approximately the

3,300 m level there is a general coarsening upward trend; above this, clast size changes little (Fig. 17).

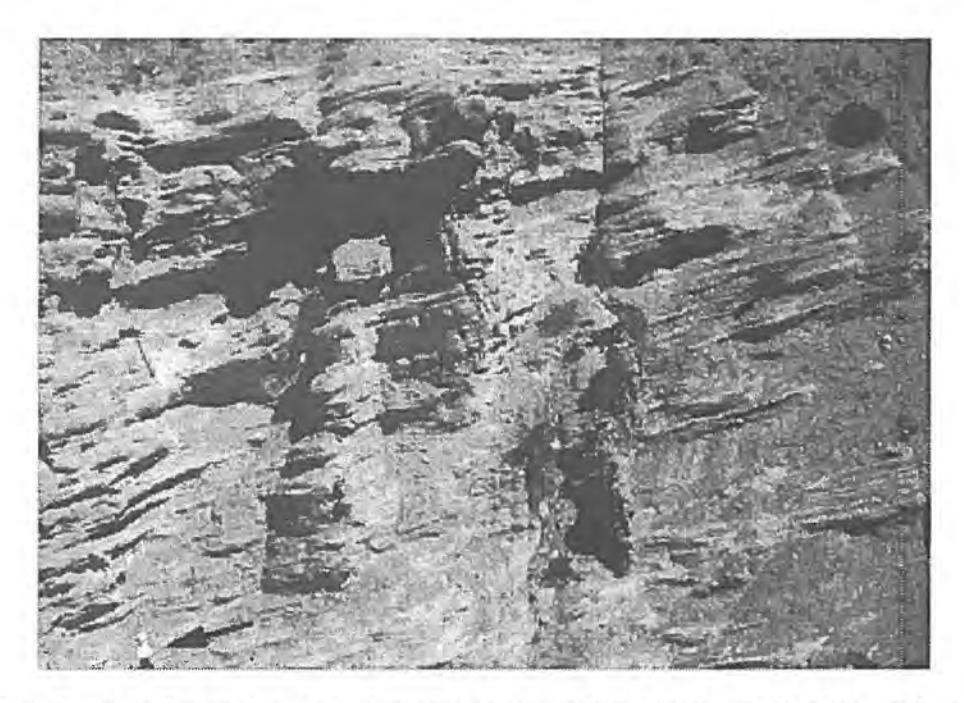


FIG. 15. Photo of cross-stratified sandstone sheets with encased sandstone and gravel ribbons near 2,725 m horizon in Group VII. These are deposits of east-flowing braided channels. Person (note arrow) for scale.



FIG. 16. Photo of conglomerate sheets near 3,400 m horizon, which are deposits of sheetfloods on an alluvial fan. Trace of bedding is gently inclined downward from left to right.

Interpretations

The authors interpret the lowermost sediments of this group to have been deposited in the distal portion of an alluvial fan where sediment transport was confined principally to narrow channels deeply incised into a fine, but poorly sorted, floodplain of a neighboring river system. The remainder of this unit accumulated on a proximal alluvial fan. The conglomerate sheets are interpreted to have been deposited during sheetflood events; the upward-fining is attributed to changing hydraulic conditions due either to flow expansion (as a result of slope change), or to changes in flow capacity (Blair and McPherson, 1994, p. 473). The ribbon conglomerates that overlie the wider concave-upward scour surfaces and cross cut the conglomerate sheets are interpreted to represent localized 'pods' of channelized flow. Blair and McPherson (1994) described a facies similar to this and interpret it to have been deposited during the upslope migration of antidunes. The authors lack information about the nature of the cross bedding within the ribbon conglomerates that would test such an interpretation. The spread of paleoflow directions, however, is consistent with flow across a fan surface and with the possibility of preserved antidunes.

The general coarsening upward nature of the lower part of the conglomeratic sequence is interpreted to indicate a progressive upward decrease in distance to the source area. The subsequent change to a constant grain size (Fig. 17) suggests deposition as the relief reached a steady state. The authors infer that individual small-scale coarsening-upward sequences (Fig. 17) (within the overall coarsening upward sequence) record fan-lobe switching.

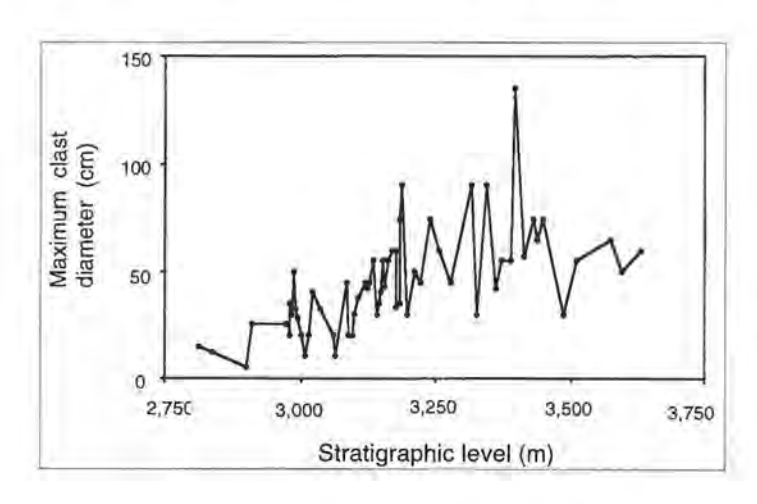


FIG. 17. The maximum diameter of the largest clasts in Group VIII increases up-section to about the 3,300 m horizon, but does not change systematically above that level.

CHRONOLOGY OF MANANTIALES SECTION

Two methods are employed to date strata in the Manantiales basin. Radioisotopic dating of interbedded volcanic ashes offers approximate dates for four horizons. Determination of the local pattern of magnetic polarity allows one to correlate horizons of reversals in polarity to the global history of magnetic reversals (Cande and Kent, 1992, 1995). Successful correlation of the local magnetic polarity history to the global time scale relies heavily on the dated ash horizons. Given the ages of many stratigraphic levels, thickness and age data were converted to a history of rates of accumulation for the section.

VOLCANIC ASH BEDS

Four volcanic ash horizons in the upper member of the Chinches Formation yielded primary ash fall deposits (Table 2). Most of these were very fine grained, but one included an horizon of coarse crystals. The samples were collected from few-centimeter-thick portions of the ash beds with no visible detrital contaminants. Mineral separations were completed at Dartmouth College, and zircons were dated by the external detector method of fission track analysis, following the methods of Naeser (1978).

The neutron dose was calibrated by C.W. Naeser (U.S. Geological Survey, Denver).

The ages range from 17.1 ± 1.9 Ma to 11.5 ± 1.4 Ma (Table 2 and Fig. 18). The ages determined for the two uppermost samples are not in correct stratigraphic order, but when the 2σ statistical uncertainty in the age of the uppermost sample (88 volc 3) is taken into account, there is no stratigraphic incon-

sistency in the results. In referring to the ages, the authors cite the range allowed by the 95% confidence level (2σ) in order to emphasize that the age range is considered to be accurate, although the precision of the mean age may be poor (Johnson *et al.*, 1979). Due to the low uranium concentrations of the zircons, the 2σ error range is necessarily large.

TABLE 2. FISSION-TRACK AGES OF INTERBEDDED ASHES.

Sample	Description	Total grains counted	Fossil density	Induced density	Age (Ma)	(Sa)
87 voic 1	ca. 50cm thickness, white bentonite	9	41,x10 ⁶	1.4x10 ⁷	17.1	1.9
88 volc 1	20 cm total thickness, lower 4 cm brown, clean bentonite	9	2.1x10 ⁶	6.2x10 ⁶	16.5	2.8
88 volc 2	45 cm total thickness, white silicified tuff; sampled 20-30 cm above base	15	1.7x10 ⁶	7.1x10 ⁶	11.5	1.4
86 voic 3	Local pod of primary ash fall; redeposited ash along strike; 9 cm total thickness locally; < 2cm basal crystal tuff overlain by 2-7cm gray bentonite	11	5,0x10 ⁵	2.0x10 ⁶	12.4	2.9

Fossil, induced, and dose densities in track/cm²; neutrondose=8.2x10¹⁴ (4094) for sample No. 88 voic 1-3 and 9.4x10¹⁴ (2750) for 87 voic 1.

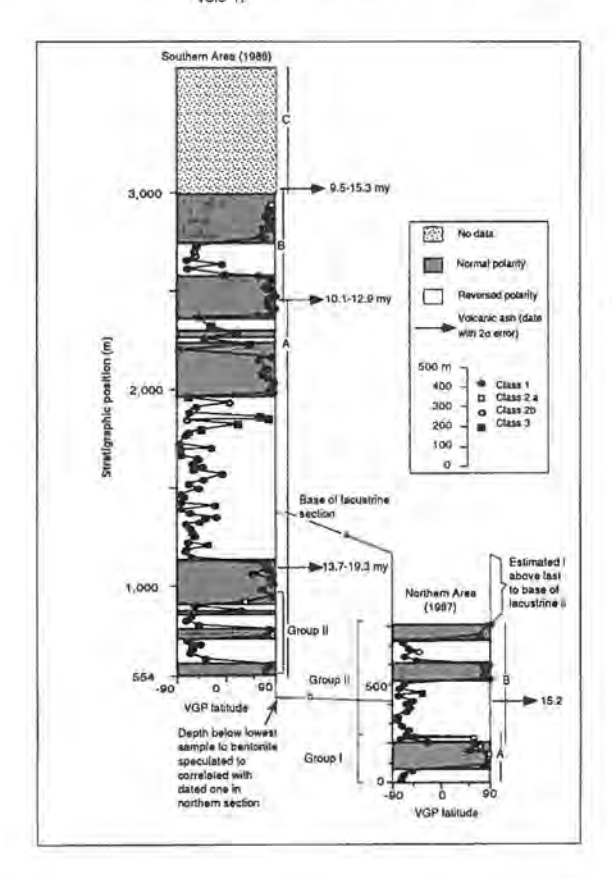


FIG. 18. Virtual Geomagnetic Pole (VGP) latitudes plotted against stratigraphic level comprise the set of symbols, whose vertical variations are synthesized to frame the local magnetic polarity column (gray and white bars). Classes indicate the degree of similarity among paleomagnetic vectors of each of the three samples at a site (data available from first author or Revista Geológica de Chile). For class 1 sites, the Fisher R value ≥2.63, class 2a sites had only 2 samples available for study, but they had R values near 2.0; class 2b sites had 3 samples with 2.0≤R<2.63, and class 3 sites had either 2 or 3 samples with little similarity among their vectors. Lines 'a' (base of lacustrine section) and 'b' (thick ash bed), and facies Groups (I and II) form bases for tentative correlation between the northern and southern sections based on recognition of similar lithologies and sequences of lithologies in both regions, and thus are independent of the magnetic correlation. Vertical lines labeled A, B, C indicate the extents of the segments of the 1987 and 1988 field sections (Fig. 3). The disputed fault that Pérez (1995) believed repeats the authors' section (FRL fault, Fig. 3) would project into the column near 1,950-2,050 m.

MAGNETIC POLARITY STRATIGRAPHY

The polarity of the earth's magnetic field at the time of deposit on of the strata was determined from laboratory measurement of oriented hand samples. Following the procedures established by Johnson et al. (1975), the authors collected three oriented samples at each of 151 sites in the lower 3,000 m of the section. Where possible, the authors sampled the preferred ithologies for paleomagnetic study: siltstone, mudstone, or fine grained sandstone. However, in several parts of the section, the finest grained material available was poorly sorted, coarse sandstone, which the authors sampled. Strata in the upper 600 m of the section were too coarse grained to obtain magnetic polarity samples. There is stratigraphic overlap between sites collected in a northern section (referred to as 1987 samples) and those from a southern section (referred to as 1988 samples). Excluding this interval of overlap, the mean stratigraphic spacing of sites is 21 m.

Paleomagnetic vectors of samples from 144 of the sites were measured with spinner magnetometers at Dartmouth College and at Syracuse University. Pilot studies of 10 samples were subjected to stepwise alternating field and/or thermal demagnetization (Fig. 19). For samples for which both alternating field and thermal demagnetizations were performed, the polarity defined by the two methods is similar (Fig. 19a, b; samples 3a and 13b), but the thermal demagnetization more effectively stripped away multiple magnetic components (Fig. 19a). Heating to 200°C removed a low-temperature normal overprint in five of the seven samples subjected to stepwise thermal demagnetization. Superimposed vector components are detected at higher temperatures, one of which is apparently stable in the temperature range from 400° to 560°C. Treatment at 575°C, approximately the Curie temperature of magnetite (Valencio, 1980), commonly resulted in a strengthening of the signal and change in vector direction. In some samples that appear to be of reversed polarity at temperatures near 540° to 560°C (e.g., Fig. 19, sample 088a), at temperatures above 575°C the vector direction is unstable. Examination of demagnetization data from additional samples (which lack systematic thermal demagnetization data for temperatures below 500°C but have several measurements between 500°C. and 650°C) further indicates that commonly magnetite and hematite carry vectors of opposed polarity.

These results, in addition to results of prior expe-

rience in the Precordillera region (e.g., Johnson et al., 1986; Reynolds et al., 1990; Jordan et al., 1990), led to a strategy of simplified demagnetization treatment for all the other samples. For all samples, the natural remanent magnetization (NRM) was first measured, and used as a baseline against which to compare the magnetic intensity after subsequent demagnetization steps. In nearly all cases, samples were analyzed again after heating to 500°C, and then analyzed after elevation to either 540°C, 560° C, and 575°C, or 550° C and 575°C. For 4% of the samples, the first thermal demagnetization step was 400°C, followed by the treatment noted above. Those samples whose magnetic intensity at 575°C exceeded 10% of the NRM were heated to 600°C, analyzed again, and if still in excess of 10% of the NRM, demagnetization continued at 640° or 650°C. The full data set may be obtained from the first author or the Revista Geológica de Chile.

The progressive thermal demagnetization data (Fig. 19) reveal that most samples carry three magnetic components: a low temperature component, magnetite and a high-temperature component (probably hematite). The polarity of magnetite is often opposite that of the low-temperature and high-temperature components. The straight demagnetization vectors pointing towards the origin on the Zijderveld vector diagrams (Fig. 19) in the temperature range of magnetite indicate that magnetite carries the most stable component, which the authors interpret as the characteristic remanent magnetization. A characteristic magnetic orientation for each sample was selected from an individual temperature step. In most cases, the authors chose temperature steps below 575°C.

Fisher statistics express the similarity between the primary magnetic components of the three samples from each site. Sites with R>2.63 are ranked as class 1 data. Sites for which one of the samples had been destroyed and only two samples could be measured, but those were nearly identical in orientation, are ranked as class 2a data. Sites with three samples, but R<2.63 and >2.00 are here treated as class 2b sites; those with R<2.00 are ranked as class 3. Sites with only a single sample were not analyzed. Of the 144 sites analyzed, 118 produced class 1 and class 2a results, and only 12 generated class 3 results. The mean orientation of mean vectors of all reversed sites is nearly antipodal with the mean orientation of all normal sites, thus fulfilling the reversal test (Fig. 20).

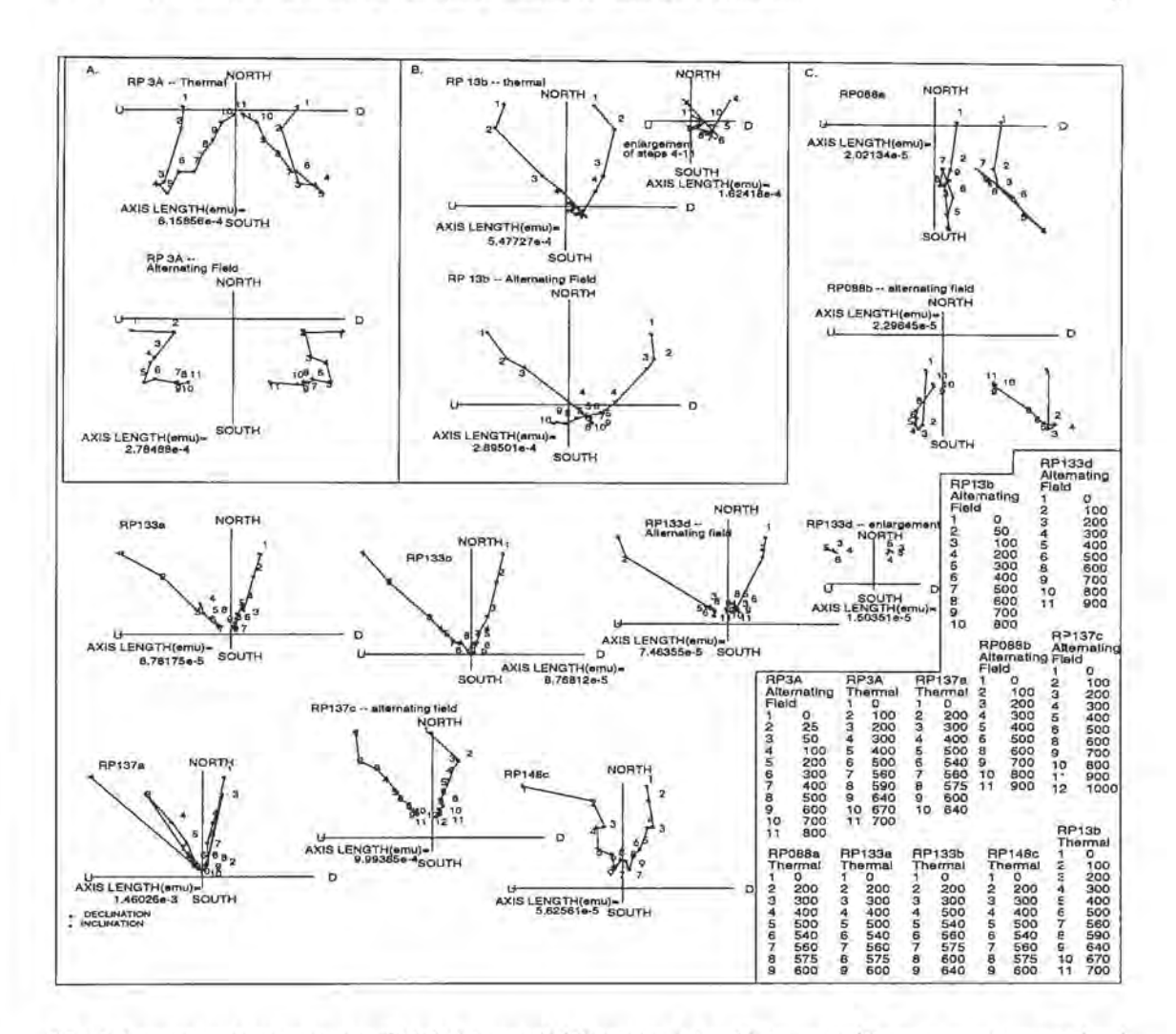


FIG. 19. Stepwise demagnetization plots (Zijderfeld diagrams) of 10 samples. In A and B, two parts of the same sample were analyzed by thermal and alternating field demagnetization. In C, results of a single type of stepwise treatment shown for each sample. Lengths of axes scaled to intensity data of samples; one axis of each plot has been cropped to save space. Numbers on plot refer to step sequence, and are keyed to data in lower right part of figure (temperatures (°C) for each thermal step, and intensity (oersteds) for each alternating field demagnetization step). U and D refer to up and down, respectively.

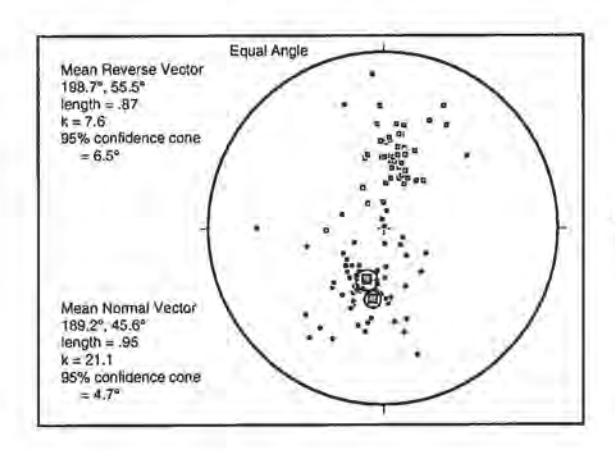


FIG. 20. Stereoplot of site mean inclinations and declinations, using only Class 1 data. Both reversed and normal data are projected onto the lower hemisphere. The Vector means of all the reversed sites have been rotated for visual comparison with the vector mean of the normal sites. The overlap of their 95% confidence cones demonstrates that the data pass the reversal test, and thus may be the record of Earth's reversing field during the time of deposition.

The local magnetic zonation (Fig. 18) is based on the polarity of stratigraphically successive sites. All, but 4 of the 18 magnetic zones have two or more successive sites of like polarity (Fig. 18). Single class 1 sites of polarity opposed to that of neighboring sites are considered to be valid evidence of a polarity zone, but single class 2 or 3 sites are not sufficient evidence of an additional polarity zone. The stratigraphic position of a reversal is considered to be half way between neighboring sites of opposed polarity. Class 2 and class 3 sites that occur at the base or top of a series of sites of like polarity are taken into consideration when selecting the stratigraphic position of a reversal (e.g., Fig. 18, polarity zone contact near 1,950 m).

Based on the existence of polarity reversals (Fig. 18) and the positive reversal test (Fig. 20), the authors conclude that the characteristic remanent magnetization is of primary origin and that the other magnetic components reveal overprints.

Because of the lack of fine-grained lithologies limited the authors to sampling coarse sandstones in parts of the section, it is useful to consider variations in the statistical validity of the paleomagnetic results as a function of grain size. Sites in strata of claystone, mudstone, siltstone, and sandstone (up to medium sand size) produced 90% class I results. In contrast, units dominated by coarse sandstones and conglomerates, in which the authors sampled lenses of poorly sorted coarse sandstone, produced only 55% class I results, with 21% class 3. Consequently, although the authors were able to maintain a regular spacing throughout the section by sampling coarser lithologies than recommended, those results are of much poorer quality.

CORRELATION TO MAGNETIC POLARITY TIME SCALE

The authors' preferred interpretation is that the local magnetic column correlates to the interval of time spanning approximately 19 to 10 Ma (chron 5) (Fig. 21). This correlation of the local magnetic polarity section to the Magnetic Polarity Time Scale (MPTS) of Cande and Kent (1992, 1995) relies heavily on independent dates provided by fission-track dating of the interbedded ashes, and is guided by the relative thicknesses of normal and reversed zones in the local column. There are three key boundary conditions employed in this correlation.

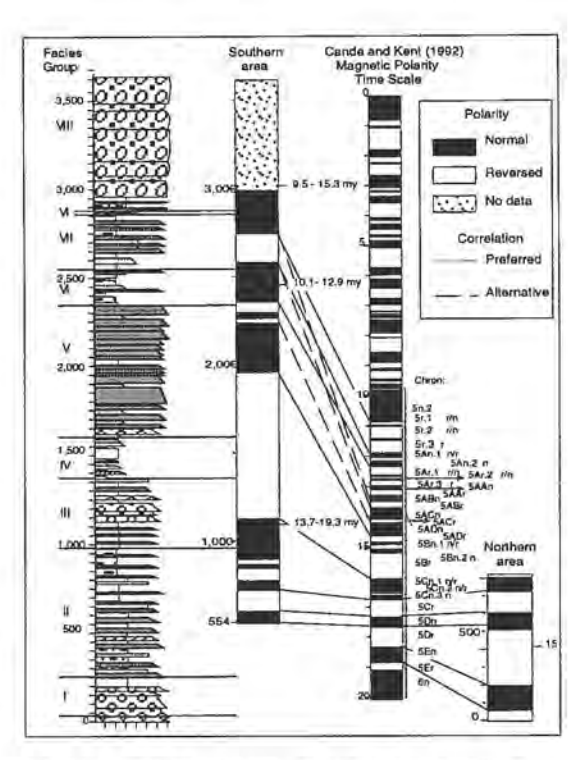


FIG. 21. Correlations of local magnetic polarity column (from Fig. 18) to Magnetic Polarity Time Scale (MPTS) of Cande and Kent (1992). For the preferred correlation (solid lines), the principal constraints are the four ash horizons with fission-track dates (shown with age range permitted by 2g error) and the long reversed polarity zone between 1,200 m and 1,950 m in column. The alternative correlation (dashed lines) places little weight on the fissiontrack dates. Stratigraphic column shown to facilitate comparisons of ages of units to facies Groups (I-VIII). The ages of polarity chrons published by Cande and Kent (1995) are slightly different from these. Specifically, near 11 Ma, Cande and Kent (1995) indicated ages 0.1 million years older, near 15 Ma the same age, and near 19 Ma ages 0.04 million years younger, than their 1992 time scale.

First, the 15.2-19.0 Ma ash at about 400 m above the base of the section occurs in a 300 m thick reversed polarity zone. The Cande and Kent (1992) MPTS shows three relatively long duration reversed polarity intervals within the time span allowed by the fission-track date: 5Br, 5Cr, 5Dr. Second, in the upper part of the column, near 2,500 m, a volcanic ash dated as 10.1-12.9 Ma occurs in a 190 m thick normal polarity zone. The MPTS contains only two potentially long-duration normal zones within the allowed time interval: 5n.2 and the combination of 5An.1 and 5An.2. The younger of these two possible correlations (5n.2) is rejected because it is inconsistent with the existence of an overlying

thick reversed zone and thick normal zone that must be older than the minimum age allowed on the highest dated ash (9.5 Ma); the only reversed zones between 9.5 Ma and 5n.2 are short duration. Third, a very thick reversed polarity zone exists in the middle of the Manantiales section (ca. 1,200-1,950 m). There may be one or more thin normal polarity zones near its top, where the section is very conglomeratic and the authors' samples yielded poor quality results (class 3 sites near 1,800 m, Fig. 18). This thick reversed interval must correlate to a time of dominantly reversed polarity of the earth's field. Given the constraints of the fission-track ages and correlations described above, the most likely interval for correlation to the MPTS is approximately 14.6-16.03 Ma (chron 5aDr through 5Br). Given the second and third boundary conditions, it follows that the thick reversed polarity zone of the northern section correlates to 5Dr. The remainder of the correlation is accomplished by comparing relative widths of normal and reversed polarity zones in the local column to relative durations in the MPTS. The major ambiguity arises for the section between about 2,000 and 2,500 m. Here there are only 5 well defined polarity zones, but the correlation strategy described above suggests that it should correlate to a time interval with 12 polarity zones. The authors interpret that there is one or more unconformities in the section in that interval, which they did not recognize in the field. This problem is discussed below.

These correlations define the accumulation history of the section (Fig. 22), from which rates of accumulation can be calculated and the age of the top of the preserved section estimated. To account for progressive compaction during burial, which would have contributed to accommodation space, the authors estimated the partially decompacted thickness through time (Fig. 22). The decompaction was performed following the equations of Sclater and Christie (1980). There is no important difference in trends of the measured-thickness accumulation curve compared to that for decompacted thicknesses.

If this correlation is correct, accumulation was relatively rapid throughout the part of the section for which the authors have magnetic polarity stratigraphy: 200 to 600 m per million years. If the rate of accumulation in the uppermost, conglomeratic, undated 600 m of the section remained the same as the long term average of the lower part of the section, the age of the top of the section would be approxi-

mately 8.7 Ma. However, if the rate were as slow as in the uppermost segment shown on figure 22, then the age of the top of the section could be as young as about 5.3 Ma. Because it is conclomeratic, one might think that the accumulation rate of the undated part of the section might be higher than those measured below. While the authors cannot disprove this assumption, available studies of other foreland basin sections reveal that, commonly, rates of accumulation are not higher in conglomeratic intervals than in sandy ones and, in general, the rates are nstead slower (Johnson et al., 1986; Reynolds et al., 1990). Below, variations in the accumulation rate over short time intervals are compared to the depositional environments.

However, the accumulation rates and all temporal information between 14.6 and 12.3 Ma are poorly resolved. This correlation of the local magnetic column to the MPTS implies that one or more unconformities exist in that interval, but the authors did not recognize those unconformities in the field. Lack of field evidence of an unconformity is noteworthy, but not conclusive, given the short time in the field and the confinement of the authors' observations to approximately 100 m of strike distance. The dominant facies in this interval, Group V, is characterized by concave-up and irregular erosive contacts between sandstone and conglomerate beds. All such surfaces represent at least short-lived unconformities: more study would be needed to differentiate among erosional surfaces related simply to reshaping bedforms and bars during changing river stage (time scale of minutes to hundreds of years) and those erosional surfaces that are related to many tens of thousands of years with no accumulation. Based on the interpretation that one or more unconformities exist between 14.6 and 12.3 Ma, the rate curve for that time span (Fig. 22) should contain intervals with rates of zero or negative accumulation (erosion). Because the poorly correlated segment of the local magnetic polarity column (upper part of Group V) is dominated by normal polarity, as is the MPTS for the older portion (14.6-13 Ma) of this time interval, the authors speculate that the unconformities lie between 13-12.3 Ma.

An alternative correlation of the ocal magnetic polarity column spans about 19 to 13.3 Ma (Fig. 21). If one chooses to treat the four fission-track dates as merely suggestive of the early and middle Miocene, but not accurate indicators of the ages of the ash

horizons, a correlation would be guided largely by the relative lengths of polarity intervals in the early and middle Miocene MPTS. The anchor point of such a correlation would again be interpretation that the long reversed zone (1,200-1,950 m) corresponds to the longest dominantly reversed interval (5ADr to 5Br). The most reasonable interpretation of the underlying magnetic zones is the same as described above. However, correlation of the upper part of the local column would differ significantly from that advocated above. The interval from 1,950 to 2,570 m is dominantly normal, apparently with two short reversed intervals (Fig. 18). It is also possible that,

rather than two short reversed intervals, there was a single longer reversed interval (*i.e.*, the low VGP normal site defining the short intervening normal (Fig. 18) is indicative of a normal overprint on a reversed polarity horizon). The authors suggest correlation of the 1,950 to 2,570 m interval to chrons 5ACn to 5ADn. If so, the uppermost normal zone in the authors' column might correlate to chron 5ABn, with no need for unconformities. Extrapolating the overall accumulation rate implied by that correlation (*ca.* 530 m per million years) to the upper 650 m of the section yields an estimated age for the top of the section of about 12 Ma.

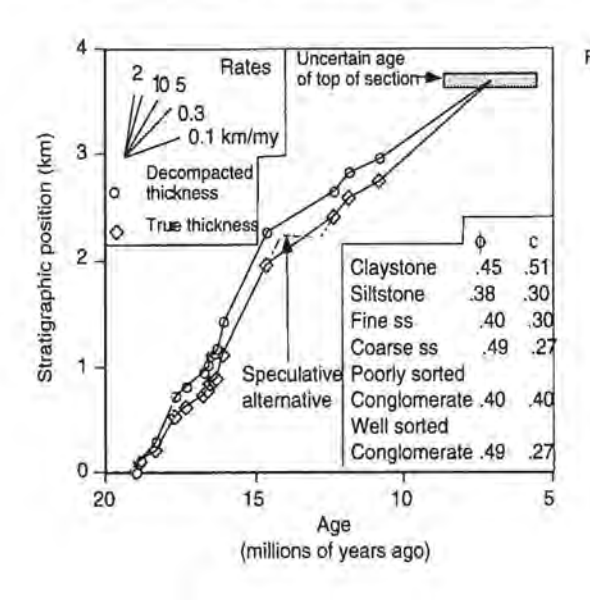


FIG. 22. History of accumulation of Manantiales basin strata, based on the preferred age model shown in figure 21. Stratigraphic positions of correlated magnetic polarity reversals are plotted against the age of the reversal. Field measurement of stratigraphic level (true thickness) and calculated thickness at the time of deposition (decompacted thickness) are each shown for each polarity reversal. Rates of accumulation at scale of figure are illustrated by inclined lines. Because the age of the top of the section is not well constrained, the authors illustrate a plausible range of ages. Dashed line indicates a speculative alternative accumulation history in the time interval with an apparent unconformity. Error bars in age are impossible to measure: they depend on the accuracy of the correlation (Fig. 21) and the accuracy of the time scale (Cande and Kent, 1992). Errors in stratigraphic position of the reversal (true thickness) are in all cases less than the vertical range of the symbols. Errors in decompacted stratigraphic position cannot be estimated meaningfully. Decompaction based on method of Sciater and Christie (1980), using lithology-dependent parameters for ø (surface porosity) and c (coefficient for the exponential rate of change of porosity with depth) shown in lower right of figure.

PETROGRAPHY OF SANDSTONES AND CONGLOMERATES

Compositions of sandstones and conglomerates can provide direct evidence of tectonic activity in a source area. The authors' data are much more extensive for sandstones (modal analyses of 23 stratigraphic leves in the lower 2,900 m of the Manantiales section) than for conglomerates. Fortunately, Pérez (1995) reported data on conglomerate clasts, which are more readily interpretable than sand grains are.

The petrography of 15 of the 23 sandstone samples was determined using thin sections stained for potassium and plagioclase feldspar (Houghton, 1980). The general composition of both groups of samples is similar, but the authors report only the details of the stained samples. The Gazzi-Dickinson (Ingersoll et al., 1984) method of point counting was used, which minimizes the extent to which varying degrees of weathering of a single source area results in variations in the sand compositions.

Sandstones in the Manantiales section are lithic arkoses and feldspathic litharenites (classification of McBride, 1963). Many of the sand grains are severely altered (e.g., albitized, calcified, sericitized, chloritized). Plagioclase and volcanic lithics are the

principal detrital clastic grains. Monomineralic grains that exceed 2% abundance are dominated by plagioclase, with lesser quantities of quartz and potassium feldspar. The lithic clasts are almost entirely of volcanic origin; within this group there are devitrified volcanic glass and grains bearing plagioclase, amphibole, and opaque phenocrysts in a fine-grained ground mass. In addition, hornblende and actinolite are common trace constituents, reaching 6% in one sample.

The dominance of volcanic-derived detrital clastic grains strongly reflects the volcanic nature of several of the potential source area units: the Permo-Triassic Choiyoi Group, Triassic rift-related volcanic units, the Cretaceous volcanic units, and the Cenozoic Farellones Formation. Most of the plagioclase grains are probably also derived from volcanic source units, as coarse phenocryst-bearing volcanic rocks break down to yield plagioclase crystals. Even the sedimentary rocks in the Principal Cordillera formed in volcanic-rich basins (Cristallini et al., 1994), and therefore they are likely to be rich in volcanic lithics and feldspars and may not yield many recycled quartz grains. Nevertheless, quartz grains are likely to indicate recycling of sedimentary source rocks as well as erosion of plutonic sources and acidic Choiyoi volcanic rocks. The authors' approach is to consider vertical trends in the suite of grains that would have come from all volcanic rocks (the sum of all the volcanic clasts and plagioclase) and in quartz (Fig. 23).

Because of the alteration of unstable mineralogies, there is considerable uncertainty in differentiating between primary grains and depositional matrix, and in recognizing the compositions at the time of deposition. To estimate that uncertainty, the authors compared the modal compositions of two sandstones that were counted twice by the same petrographer (TC). In each grain category (Fig. 23), a minimum value of uncertainty is given by the difference between the two counts (shown as length of heavy horizontal lines). The authors took the maximum of those uncertainties for each grain category (e.g., 7% for quartz, Fig. 23), and used that as a plausible error bar for the remainder of the samples (thin lines).

Sandstone compositions vary little through the section (Fig. 23). The percentage of the volcanic-derived suite (including plagioclase) exceeds 65% in all the samples. A variation in excess of the error bars occurs only near 1,300 m, where a single

sample is especially rich in the volcanic-suite composition. Quartz grains constitute less than 15% of any of the samples. Between approximately the 2,000 m and 2,400 m levels in the section (14.5-12.3 Ma, using the authors' preferred correlation), plagioclase grains are considerably more abundant and all other volcanic clasts much less abundant than in underlying and overlying strata.

One possible interpretation of the large increase in plagioclase and decrease in volcanic sand grains during the interval with problematic dates (14.5-12.3 Ma) is that they represent deeper weathering of the source regions. Increased weathering might be an expression of decreased topographic relief, due to a decline in tectonic activity. Alternatively, it might also reflect climate change, such as a time of warmer

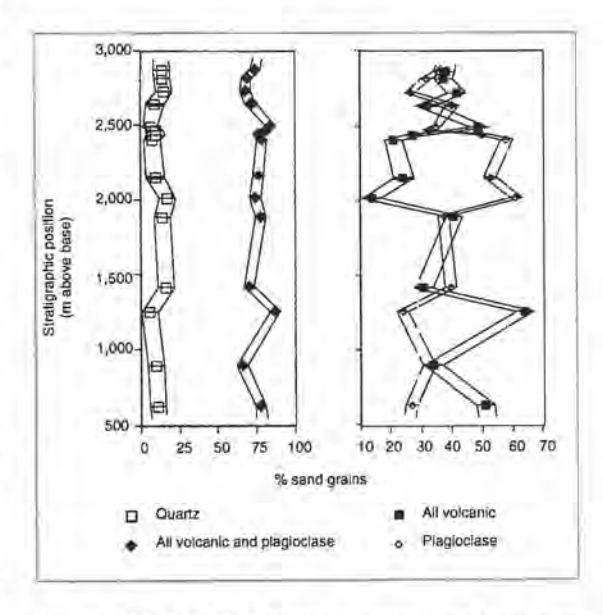


FIG. 23. Vertical trends in sandstone compositions. Error bars: thick lines indicate samples for which replicate point counts available; thin lines indicate uncertainty estimated from other horizons (for plagloclase 3%, quartz 7%, all volcanic clasts 6%, and all volcanic clasts plus plagloclase 3%). Error estimated for all volcanic rocks and plagloclase is approximately width of symbol.

climate and more chemical weathering.

Pérez (1995) studied modal compositions of conglomerates in the basin and identified the bedrock units from which they were derived. He reported conglomerate compositions for three sections. One of his sections (Aldeco) lies 1 km north of the main

transect of the authors' 1988 section; a second section (Pérez's Leñas section) lies about 7 km south of the authors' 1988 section. Based partly on the fact that the Aldeco and Leñas sections differ in their positions relative to modern drainages, Pérez (1995) speculated that, in the Miocene, the Leñas section lay near the course of a river which drained a large area west of Cordón del Espinacito, whereas the Aldeco section lay adjacent to minor, short headed drainages.

Although Pérez's (1995) data cannot be unambiguously correlated to the authors' section due to large inconsistencies in measured unit thicknesses and interpretations of fault repetition, some general comparisons are possible (Fig. 24). In addition to several categories of volcanic rocks, which in sum constitute the majority of clasts, Pérez (1995) reported that limestone clasts and red sandstones occur throughout the entire section. In the lowest few hundred meters of the Aldeco section, rhyolites and granites derived from the Choiyoi Group comprise more than 50% of the clasts, then diminish to 40% through the next interval (roughly 18-16 Ma),

but increase to near 70% in Group IV (roughly 15.7-15 Ma), which is the lower lacustrine interval. In his Aldeco section, this is overlain by a second cycle of varying Choiyoi-derived clast abundances: Group V rocks contain near 50% rhyolite, followed by values near 70% in the authors' Group VI (near 12 Ma), which is the second lacustrine interval (Pérez, 1995, Fig. 61). The percentage of clasts attributed to Miocene andesitic source rocks is also greater in the lower lacustrine interval than in overlying and underlying strata. In fact, Pérez (1995) reported only clasts of Miocene andesites and Choiyoi rhyolites in the lower lacustrine unit in the Aldeco section. In the Leñas section, the lower lacustrine interval is again exceptionally rich in Choiyoi-derived clasts, but the upper lacustrine interval (Group VI) is not enriched in Choiyoi clasts but instead in limestones (Pérez, 1995, Fig. 60). For the uppermost conglomeratic interval (Group VIII) in both sections, units whose clasts equal or exceed 10% in many horizons include Choiyoi rhyolites, Triassic-Jurassic ashes, and Jurassic limestones and red sandstones (Pérez, 1995).

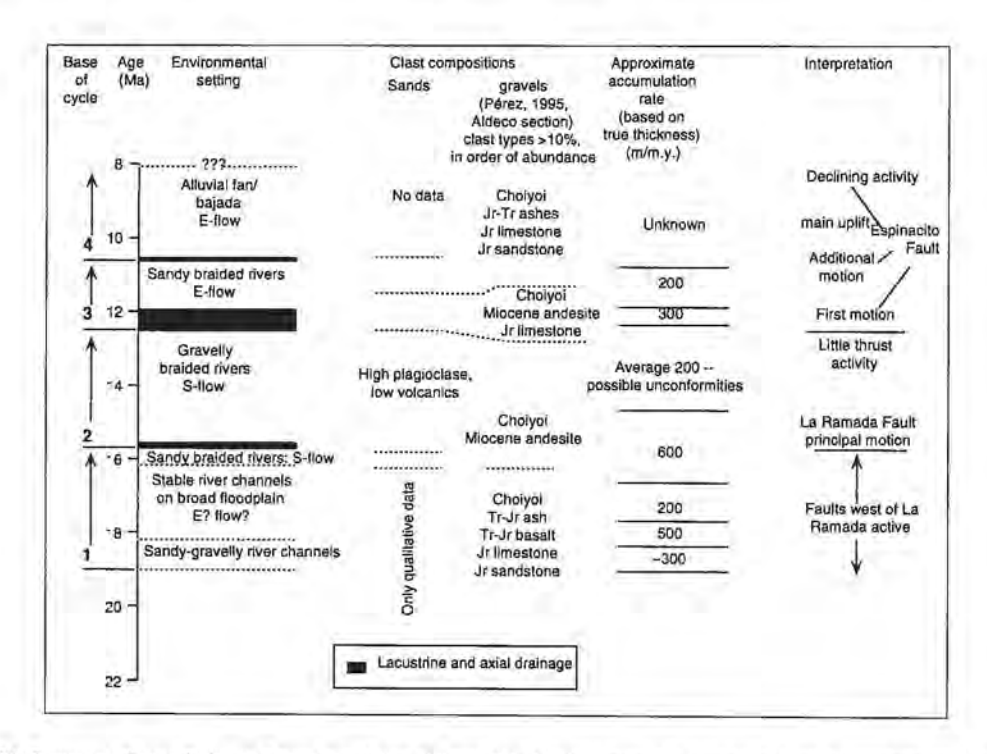


FIG. 24. Summary of ages (using preferred correlation of figure 21) of facies cycles 1-4, variations in clast petrology, and accumulation rate changes, from which the authors derive an interpretation of the history of thrusts in the La Ramada thrust belt.

DISCUSSION AND INTERPRETATION OF ENVIRONMENTAL CYCLES

The combined information about depositional environment, rates of accumulation, and provenance of the Manantiales basin allows an improved understanding of the history of thrusting in the Cerro Aconcagua-La Ramada fold and thrust belt. Here the authors describe their interpretation strategy and translate the information presented above to an absolute time scale (Fig. 24).

Of the available types of information, the depositional environments are probably most sensitive to thrust activity, but the link between depositional environment and thrust activity is difficult to interpret correctly. The difficulty with interpretation stems from the fact that multiple causes interact to determine discharge of river systems and slopes of the depositional surface (e.g., Paola et al., 1992; Jordan et al., 1988). Nevertheless, one important motif of tectonically driven environmental cycles consists of a vertical sequence that begins with lake deposits and coarsens upward to fluvial or alluvial fan facies (e.g., Blair and Bilodeau, 1988; Heller et al., 1988). Such cycles reflect the interaction of temporally varying rates of tectonic subsidence with temporally varying sediment flux.

Flemings and Jordan (1990; Jordan and Flemings, 1990) modeled the stratigraphic response in a foreland basin to episodic movement on a thrust. The models predict that initiation of a phase of thrust activity results in tectonic subsidence in excess of sediment supply, which produces a sharply defined topographic axis within the depositional basin, close to the thrust front. As thrust activity is maintained, sediment supply increases, causing basin-margin facies to prograde and the basin axis to shift away from the deformation front. During times of no thrust activity, rates of subsidence are low and the basinmargin facies spread broadly across the foreland basin. The theoretical models also predict that proximal and distal sites will differ in the pattern of changing accumulation rates through a cycle of thrust activity (Flemings and Jordan, 1990; Jordan, 1995). In parts of the basin near the thrust front, accumulation rates increase when thrusting begins, peak while the thrust is active, and decline during times of thrust quiescence. However, at sites distant from the thrust front, the rate of accumulation increases when thrust activity decreases, because

that is the time at which proximal subsidence ceases to trap sediment and it is passed to distal sites. In summary, although **tectonic** subsidence throughout the basin is simultaneous with times of thrust thickening, the accumulation of strata is not a strict record of local tectonic subsidence and **accumulation** rates must be interpreted carefully.

Due to a- a real thrust belt has more than one thrust fault; b- climate change affects discharge, and c- inherited rock properties affect subsidence, these theoretical models do not allow the authors to make a complete, detailed interpretation of thrust history based on the stratigraphy of a true foreland basin. Nevertheless, the Manantiales basin provides a case in which stratigraphy can be compared to the models.

The Manantiales basin in the ⊃ampa Negra section displays 4 major environmental cycles (Fig. 24), which (for the preferred age correlation, Fig. 21) begin at approximately 19 Ma, 15.7 Ma, 12.5 Ma, and 10.5(?) Ma. The upper three cycles begin with lake deposits and coarsen upward. The basal cycle initiates with the unconformity at the top of the andesitic breccia and has no lake facies. Because lakes are an unambiguous indicator of a topographic axis, the authors interpret that each of the upper three cycles reflects a changing basin morphology; there was an early form with a topographic axis at the Pampa Negra site, but progressively the supply of sediment from western sources filled that early axis and caused it to shift to the east. The authors interpret that each of these cycles is analogous to the tectonically-driven environmental cycles described by Blair and Bilodeau (1988), Heller et al. (1988) and Flemings and Jordan (1990). For the first cycle, there is no clear indication of a topographic low defining a basin axis.

Pérez's (1995) conglomerate data (Fig. 24) and the authors' sandstone data (Fig. 23) appear to be in agreement and to indicate that the largest shift in source area occurred when the lower interval of lacustrine interbeds began to accumulate (roughly 15.7 Ma). Prior to that time, the variety of clast lithologies indicates sources in many units exposed west of Cordón del Espinacito (Pérez, 1995), carried to the basin in east-draining rivers. The participation of clasts derived from Triassic-Jurassic rift basin

facies (ashes and basalts) (Pérez, 1995) indicated that at least part of the source area lay west of the fault that now bounds the eastern flank of Cordón de la Ramada (Fig. 2). However, at approximately 15.7 Ma those rivers were diverted or truncated, and only clasts from Miocene volcanic rocks and Choivoi Group were supplied to the basin for the duration of the interval with lacustrine interbeds. Present distribution of rock types implies that Miocene volcanic and Choiyoi clasts could be supplied by either Cordón de la Ramada or Cordón del Espinacito (Fig. 2), but the small set of chronological data available does not ident fy volcanic rocks old enough to have sourced these clasts (Pérez, 1995). The subsequent return of a mixed variety of clasts, especially at southern sites in the basin (Pérez, 1995), suggests that east-flowing rivers again tapped part of the western flank of the Cordón de la Ramada. A second. less marked, event of stream diversion or truncation accompanied the second lacustrine interval (approximately 12.5 Ma).

Rates of accumulation are indicators of relative changes in the summed subsidence rate and sediment flux. Because of the authors' rate data are tied to the magnetic polarity stratigraphy, they are limited in resolution by the natural spacing of magnetic reversals in the magnetic polarity time scale (Fig. 21). Although the resolution of rates is irregular through the section, between 19 and 14.6 Ma and again between 12.3 and 10.8 Ma, rate estimates are available for most polarity intervals.

As a test of the authors' contention that environmental cycles reflect episodes of tectonic activity, it would be des rable to compare accumulation rates to environments of deposition. If the Flemings and Jordan (1990)'s model is a correct basis for interpreting the environmental cycles, whereby the lake facies are the bases of cycles and indicate times of high rates of thrust activity, then one would predict that accumulation rates would be low in the lower zone of lake facies, high in the upper zone of and immediately above the lake facies, and lower at the tops of environmental cycles. Such a comparison is possible for the third cycle.

The third environmental cycle initiates with lacustrine deposits at approximately 12.5 Ma, lake deposits alternate with deposits of large south-flowing trunk river systems until approximately 11.9 Ma, and then the cycle coarsens upward through sandy braided river facies until approximately 10.5 Ma. If the authors' interpretation of the 14.6 to 12.3

Ma interval is correct, then accumulation in the time interval immediately preceding this lake was very slow or zero (Figs. 22, 24). The rate of accumulation was high (300 m/my) from approximately 12.3 to 11.8 Ma, an interval that nearly coincides with the lake and trunk stream environment. The rate decreased to ca. 200 m/my in the interval with braided east-flowing rivers that cap the cycle. The authors conclude that the combination of this environmental cycle and the rates of accumulation support use of the Flemings and Jordan (1990) model of facies response to episodic thrust activity.

In contrast, the resolution of rate information is not adequate to establish a correlation between rate and various stages in the underlying environmental cycle. In that case, the cycle began at approximately 15.7 Ma with a stacked series of six intervals of lacustrine mudstones alternating with lake margin and fluvial deposits, and then continued with coarsening upward braided stream facies until 12.3 Ma. Although the lakes existed during a time that clearly had a high rate of accumulation (600 m/my), the nearly 1.5 million years between dated horizons preclude relating the high rate specifically to a particular zone in the environmental cycle (Figs. 22, 24).

In addition to the interpretations of tectonic controls on facies highlighted above, it must be recognized that the time interval defined by the authors' chronological studies is one of considerable global climate change. Specifically, according to Flower and Kennett (1994, adjusted to the Cande and Kent (1992) time scale), between ca. 16-14.6 Ma, global climate was transitional from a prior condition of relatively stable warmth to later cold, with large short term variations. Between ca. 14.6 and 12.7 Ma, the East Antarctic ice sheet grew markedly (Flower and Kennett, 1994). Although no glacial deposits in the Andes older than 7 Ma (Mercer, 1983) have been dated, it is reasonable to speculate that mountain glaciers formed in high altitude zones of the Central Andes while the Antarctic ice sheet expanded in the middle Miocene. The authors do not know whether the La Ramada thrust belt attained sufficient elevation during the middle Miocene to be glaciated, nor is there any direct evidence of such glaciation. Nevertheless, there is the likelihood that the Principal Cordillera headwaters of the Manantiales basin were subject to fluctuations in discharge and input sediment properties (grain size and compositions) due to variable climate.

Pérez (1995) reported the palynological asso-

ciation found in lacustrine claystones and siltstones of Group IV. The flora indicate a comparatively warm, dry climate associated with a shallow lake. Interestingly, the microforaminifera planispirals were identified in the same sample, which Pérez (1995) reported, indicates a marine influence. He correlated this marine incursion with the Paranense transgres-

sion that affected much of northern and western Argentina (Windhausen, 1931). Given the authors' interpretation of the stratigraphy and structure of the Pampa Negra section (which differs from that of Pérez's, 1995), the age of the marine transgression of the Manantiales basin is near 15-16 Ma.

TECTONIC SYNTHESIS

The authors synthesize the preceding interpretations in reference to the structural geology of the La Ramada portion of the Principal Cordillera thrust belt as follows. The most compelling relationship between thrusting and stratigraphy is the most general: the Manantiales basin strata began to accumulate when thrusting began in the La Ramada thrust belt, and continued to accumulate throughout the interval of deformation. Furthermore, the dated strata are all rotated, so thrusting continued after deposition of the preserved horizons. The age of the base of the section where exposed along the current position of the Río de los Patos may be younger than the age of initial thrusting, and represents the time at which the wedge of sediment derived from the thrust belt prograded across a rather distal part of the basin. Thus, the La Ramada thrust belt was active during the interval spanning 19-10 Ma, and perhaps as recently as 8 to 5 Ma.

The authors' data permit identification of the times of thrust activity with much more confidence than the positions of those thrusts. Episodes with active thrusting followed by little (or more distant) shortening initiated prior to 19.0 Ma, and at approximately 15.7 Ma, 12.0 Ma and 10.5 Ma.

The authors attribute the basin development between 19 and about 15.7 Ma to thrusting and uplift in what is now the western part of the thrust belt (clast compositions suggest that it involved Cordón del Medio and the western flank of Cordón de la Ramada, Fig. 2). The development of a sharp basin axis, expressed by ponding of lake sediments, and change in provenance beginning at 15.7 Ma suggest that a new phase of thrust activity had begun. They also suggest that the position of the thrust load had shifted markedly eastward, closer to the Pampa Negra section position. Because of the La Ramada thrust deforms, considerable areas of the Choiyoi Group and its trace lie only about 30 km west of the

authors' section (Fig. 2), it is a candidate for the thrust whose activity began at 15.7 Ma. The 10.7±0.7 Ma subhorizontal volcanic rocks overlying folded units in the La Ramada structural block are consistent with this interpretation of the La Ramada thrust (S.M. Kay, personal communication, 1996.)

The lacustrine-based cycle that began at approximately 12.5 Ma again coincided with a disruption of paths of sediment delivery, which the authors interpret to mean that another topographic barrier, probably Cordón del Espinac to, was generated between the older source area and the basin. Although Pérez (1995) concluded that most of the deformation of Cordón del Espinacito predated 12.7±0.6 Ma subhorizontal volcanic units, the authors' conclusions are compatible if either the analytical uncertainties in Pérez's age of the andesites or the uncertainty in the age of the base of this lacustrine cycle are taken into consideration, and if those volcanic rocks pin the principal local rotation of the Espinacito hangingwall, but not its entire translation. The subsequent development of an east-flowing set of rivers and appearance of progressively coarser conglomerates is indicative of a distance between the mountain front and the authors' site in the Manantiales basin that is shorter than it was in the underlying cycles. The last facies cycle, although it begins with lake deposits as two of the older cycles did, involves a thinner interval of lacustrine deposits and little overall difference in the facies that overlie and underlie those lake deposits. The authors interpret that, in contrast to the cycle that underlies it, the uppermost cycle represents a minor modification of the basin, perhaps caused by a minor reactivation of shortening on a thrust set, but not a large step in the position of the active thrusts. The top of that cycle includes the extremely coarse boulder conglomerates that today lie at the foot of Cordón del Espinacito and that almost certainly were produced

from that mountain front. Thus, the thrust responsible for the topmost cycle is almost certainly the Espinacito fault also.

If one rejects the fission-track dates on the ashes and accepts the alternative correlation (Fig. 21), the second and third lacustrine-based cycles would have begun near 14 and 13.3 Ma. The interpreted age of deformation of Cordón del Espinacito would then be about 14 to 12 Ma.

In summary, the authors' preferred interpretation is that the western thrusts of the La Ramada thrust belt became active at or before 19 Ma, the eastern margin of deformation shifted to the La Ramada thrust at about 15.7 Ma, and then again shifted to the Espinacito thrust at about 12.5 Ma. Thrusting continued until a time more recent than 10.5 Ma, the age of the youngest horizon that the authors can date with their methods. The authors extrapolate that the top of the Manantiales basin strata could be as young as 8.7 to 5.3 Ma. The youngest thrusting is younger than the top of the section (Pérez, 1995). Given slow accumulation and/or erosion between ca. 14 and 12.5 Ma, this may have been a short interval with little or no thrust activity. Structural geological reconstructions (Cristallini et al., 1994) indicate that the older, western thrusts may be truly thin-skinned, with shallow 'décollements', but that the major faults, which the authors interpret to have been active between 15.7 Ma and younger than 10.5 Ma, were a system of thrusts that penetrate or sole into the Choiyoi basement.

This history of thrust activity is similar to the more generalized chronology established by Ramos et al. (1990) for the Cerro Aconcagua latitude of the thrust belt (Fig. 4). The early Miocene initiation of deformation preceded deformation of the Frontal Cordillera 100 km farther north (Maksaev et al., 1984), but is similar in age to first thrusting in the Precordillera (Jordan et al., 1993a). Although 14 to 12.5 Ma is an interval in which thrust activity may have waned or ceased in the La Ramada belt, this does not necessarily indicate a lack of shortening in the entire orogenic belt, given likely thrusting in the Precordillera to the east (Bercowski et al., 1993; Jordan et al., 1993a).

This interpretation of the thrust history differs markedly from that of Sempere et al. (1994), who concluded that the major phase of thrust activity occurred between 27 and 20 Ma. Although deformation may have occurred between 27 and 20 Ma in the La Ramada thrust belt, the authors presume that it was less important than that between 19 and 10 Ma, based on the volume of lower and middle Miocene foreland basin strata.

ACKNOWLEDGEMENTS

The authors fondly acknowledge the collaboration of the late N.M. Johnson and D. Johnson (Dartmouth College) in the early phase of paleomagnetic studies. L. McRae (Dartmouth College), P. Plumley (Syracuse University), B. Urma, (Syracuse University and Cornell University), M. Koh (Cornell University), and B. MacFadden (University of Florida) all assisted the authors in laboratory analyses and interpretation of the paleomagnetic data. J. Damanti (Union College) contributed initial petrographic studies. Discussions of structural geology and volcanic history with R.

Allmendinger (Cornell University), V. Ramos (Universidad de Buenos Aires), S.M. Kay (Cornell University), and C. Mpodozis (SERNAGEOMIN), logistical collaboration with F. Bercowski (Universidad Nacional de San Juan), R. Allmendinger, and the gendarmes at Alvarez Condarco, and critical reviews by F. Schlunegger (Cornell University), V. Ramos and P. Roperch (ORSTOM-Universidad de Chile) were much appreciated. Financial support provided by NSF grants EAR 8617035, EAR 8904537, and GER 9022811 awards to one of the authors (TJ).

REFERENCES

Allen, P.A.; Allen, J.R. 1990. Basin Analysis; principles and applications. *Blackwell Scientific Publications*, 451 p. Oxford.U.K.

Alvarez, P.; Pérez, D.J. 1993. Estratigrafía y estructura de

las nacientes del Río Colorado, Alta Cordillera de San Juan. In Congreso Geológico Argentino, No. 12, y Congreso de Exploración de Hidrocarburos, No. 2, Actas, Vol. 2, p. 78-84. Mendoza.

- Baldis, B.A.; Martínez, R.; Villegas, C.R.; Pereyra, M.E.; Pérez, A.M. 1990. Estructura, provincialismo geológico y unidades tectonoestratigráficas. Relatorio de Geología y Recursos Naturales de la Provincia de San Juan, p.186-211.
- Beaumont, C. 1981. Foreland basins. Geophysical Journal of the Royal Astronomical Society, Vol. 65, No. 2, p. 291-329.
- Bercowski, F.; Ruzycki, L.; Jordan, T.; Zeitler, P.; Caballero, M.M.; Pérez, I.1993. Litofacies y edad isotópica de la secuencia La Chilca y su significado paleogeográfico para el Neógeno de Precordillera. In Congreso Geológico Argentino, No. 12 y Congreso de Exploración de Hidrocarburos, No. 2, Vol. 1, p. 212-217. Mendoza
- Blair, T.C.; Bilodeau, W.L. 1988. Development of tectonic cyclothems in rift, pull-apart, and foreland basins; sedimentary response to episodic tectonism. *Geology*, Vol. 16, No. 6, p. 517-520.
- Blair, T.C.; McPherson, J.G. 1994. Alluvial fans and their natural distinction from rivers based on morphology, hydraulic processes, sedimentary processes, and facies assemblages. *Journal of Sedimentary Research*, Vol. A64, No. 3, p. 450-489.
- Cande, S.C.; Kent, D.V. 1992. A new geomagnetic polarity time scale for the Late Cretaceous and Cenozoic. *Journal of Geophysical Research*, Vol. 97, No. B10, p. 13917-13951.
- Cande, S.C.; Kent, D.V. 1995. Revised calibration of the geomagnetic polarity time scale for the Late Cretaceous and Cenozoic. *Journal of Geophysical Research*, Vol. 100, No. B4, p. 6093-6095.
- Cegarra, M.I.; Lo Forte, G.L.; Sanguinetti, A.S. 1993. La Alta Cordillera de Mendoza entre Puente del Inca y Las Cuevas (32° 50' Lat. S). In Congreso Geológico Argentino, No. 12 y Congreso de Exploración de Hidrocarburos, No. 2, Actas, Vol.2, p. 85-93. Mendoza.
- Charrier, R.; Wyss, A.R.; Flynn, J.J.; Swisher, C.C. III; Spichiger, S.; Zapatta, F. 1994. Nuevos antecedentes estratigráficos para las formaciones Coya-Machalí y Abanico, entre 33°50' y 35° Cordillera Principal Chilena. In Congreso Geológico Chileno, No. 7, Actas, Vol. 2, p. 1316-1319. Concepción.
- Cortés, J.M. 1993. El frente de corrimiento de la Cordillera Frontal y el extremo sur del Valle de Uspallata, Mendoza. In Congreso Geológico Argentino, No. 12 y Congreso de Exploración de Hidrocarburos, No. 2, Vol. 3, p. 168-178. Mendoza.
- Cristallini, E.O.; Mosquera, A.; Ramos, V.A. 1994. Estructura de la Alta Cordillera de San Juan: Evidencias de inversión tectónica, Asociación Geológica Argentina, Revista, Vol. 49, p. 165-183.
- Flemings, P.B.; Jordan, T.E. 1990. Stratigraphic modelling of foreland basins: interpreting thrust deformation and lithospheric rheology. *Geology*, Vol. 18, No. 5, p. 430-435.
- Flower, B.P.; Kennett, J.P. 1994. The middle Miocene climatic transition: East Antarctic ice sheet develop-

- ment, deep ocean circulation and global carbon cycling. InCenozoic climate and paleogeographic changes in the Pacific region (Cronin, T.M.; editors; et al.). Palaeogeography, Palaeoclimatology, Palaeoecology, Vol. 108, No. 3-4, p. 537-555.
- Heller, P.L.; Angevine, C.L.; Winslow, N.S.; Paola, C.1988.
 Two-phase stratigraphic model of foreland basin sequences. Geology, Vol. 16, No. 6, p. 501-504.
- Homewood, P.; Allen, P.A.; Williams, G.D. 1986. Dynamics of the Molasse Basin of western Switzerland. In International Association of Sedimentologist, Special Publication, Vol. 8, p. 199-217.
- Houghton, H.F. 1980. Refined techniques for staining plagioclase and alkali feldspars in thin sections. *Journal* of Sedimentary Petrology, Vol. 50, No. 2, p. 629-631.
- Ingersoll, R.V.; Bullard, T.F.; Ford, R.L.; Grimm, J.P.; Pickle, J.D.; Sares, S.W. 1984. The effect of grain size on detrital modes: a test of the Gazzi-Dickinson pointcounting methods. *Journal of Sedimentary Petrology*, Vol. 54, No. 1, p. 103-116.
- Johnson, N. M.; Jordan, T. E.; Johnsson, P. A.; Naeser, C. W.1986. Magnetic polarity stratigraphy, age and tectonic setting of fluvial sediments in an eastern Andean foreland basin, San Juan Province, Argentina. In Foreland basins (Allen, P.A.; Homewood, P.; editors). International Association of Sedimentologists Special Publication, Vol. 8, p. 63-75.
- Johnson, N. M.; Opdyke, N. D.; Lindsay, E. H.1975. Magnetic polarity stratigraphy of Pliocene-Pleistocene terrestrial deposits and vertebrate faunas, San Pedro Valley, Arizona. Geological Society of America Bulletin, Vol. 86, No. 1, p. 5-12.
- Johnson, N.M.; McGee, V.E.; Naeser, C.W. 1979. A practical method of estimating standard error of age in the fission track dating method. *Nuclear Tracks*, Vol. 3, No. 3, p. 93-99.
- Jordan, T.E. 1981. Thrust loads and foreland basin evolution, Cretaceous, western United States. American Association of Petroleum Geologists, Bulletin, Vol. 65, p. 2506-2520.
- Jordan, T.E. 1995, Retroarc Foreland and Related Basins. In Tectonics of Sedimentary Basins (Ingersoll, R.V.; Busby, C.; editors). Blackwell Scientific Publications, p. 331-362.
- Jordan, T.E.; Flemings, P.B.1990. Análisis teórico de la estratigrafía de cuencas de antepaís durante deformaciones episódicas. Reunión Argentina de Sedimentología, No. 3, Actas, p. 151-162. San Juan.
- Jordan, T.E.; Drake, R.E.; Naeser, C.1993b. Estratigrafía del Cenozoico medio en la Precordillera a la latitud del Río Jachal, San Juan, Argentina. In Congreso Geológico Argentino, No. 12 y Congreso de Exploración de Hidrocarburos, No. 2, Vol. 2, p. 132-141. Mendoza.
- Jordan, T.E.; Allmendinger, R.W.; Damanti, J.F.; Drake, R.E. 1993a. Chronology of motion in a complete thrust belt: the Precordillera, 30-31°S, Andes Mountains. Journal of Geology, Vol. 101, No. 2, p. 135-156.

- Jordan, T.E.; Rutty, P.M.; McRae, L.E.; Beer, J.A.; Tabbutt, K.; Damanti, J.F. 1990. Magnetic polarity stratigraphy of the Miocene Río Azul section, Precordillera thrust belt, San Juan province, Argentina: In Chronostratigraphy of Cenozoic terrestrial sediments and faunas (MacFadden, B.J.; editor). Journal of Geology, Vol. 98, No. 4, p. 519-539.
- Jordan, T. E.; F emings, P. B.; Beer, J. A. 1988. Dating of thrust-fault activity by use of foreland-basin strata. In New perspectives in basin analysis (Kleinspehn, K.; Paola, C.; editors), in the collection Frontiers in sedimentary petrology. Springer-Verlag, p. 307-330. New York.
- Kozlowski, E.E.; Manceda, R.; Ramos, V.A. 1993. Estructura. In Relatorio, Geología y Recursos Naturales de Mendoza (Ramos, V.A.; editor). In Congreso Geológico Argentino, No. 12 y Congreso de Exploración de Hidrocarburos, No. 2, p. 235-256. Mendoza.
- Lencinas, A.N. 1982. Características estructurales del extremo sur de la Cordillera Sanjuanina, Argentina. In Congreso Latinoamericano de Geología, No. 5, Actas, Vol. 1, p. 489-498. Argentina.
- Maksaev, V.; Moscoso, R.; Mpodozis, C.; Nasi, C. 1984. Las unidades volcánicas y plutónicas del Cenozoico superior en la alta cordillera del Norte Chico (29°-31°S): Geología, alteración hidrotermal y mineralización. Revista Geológica de Chile, No. 21, p. 11 -51.
- McBride, E.F. 1963. A classification of common sandstones. *Journal of Sedimentary Petrology*, Vol. 33, p. 664-669.
- Mercer, J.H. 1983. Cenozoic glaciation in the southern hemisphere. Earth and Planetary Sciences, Annual Reviews, Vol. 11, p. 99-132.
- Milana, J.P.; Cevallos, M.F.; Zavattieri, A.M.; Prampano, M.; Papu, H.O. 1993. La secuencia terciaria de Pachaco: sedimer tología, edad, correlaciones y significado paleogeográfico. In Congreso Geológico Argentino, No. 12 y Congreso de Exploración de Hidrocarburos, No. 2, Actas, Vol.1, p. 226-234. Mendoza.
- Mirré, J.C. 196€. Geología del Valle del Río de los Patos (entre Barreal y Las Hornillas). Revista de la Asociación Geológica Argentina, Vol. 21, No. 4, p. 211-231.
- Munizaga, F.; Vicente, J. C. 1982. Acerca de la zonación plutónica y del volcanismo miocénico en los Andes de Aconcagua (lat. 32-33°S): datos radiométricos K-Ar. Revista Geológica de Chile, No.16, p. 3-21.
- Naeser, C.W. 1976. Fission track dating. U.S. Geological Survey, Open-File Report, No. 76-19, p. 1-68.
- Paola, C.; Heller, P.L.; Angevine, C.L. 1992. The largescale dynamics of grain-size variation in alluvial basins, 1: theory. *Basin Research*, Vol. 4, p. 73-90.
- Pérez, D.J. 1995. Evolución geológica de la región del Cordón del Espinacito, Provincia de San Juan, Argentina. Ph.D. Tesis (Inédito). Universidad de Buenos Aires, Departamento de Ciencias Geológicas, 262 p.
- Ramos, V.A.; Oegarra, M.; Cristallini, E. (In press). Cenozoic tectonics of the High Andes of west-central Argentina

- (30°-36°S latitud). Tectonophysics.
- Ramos, V.A.; Aguirre-Urreta, M.B. 1991. La discordancia primordial del Valle Hermoso, Alta Cordillera de San Juan, Argentina: reinterpretación tectónica. *In Con*greso Geológico Chileno, No. 6, Actas, Vol 1, p. 887-891. Viña del Mar.
- Ramos, V.A.; Pérez, D.; Aguirre-Urreta, M.B. 1990. Geología del Filo de Zürbriggen, Aconcagua, Mendoza. In Congreso Geológico Argentino, No. 11, Actas, Vol. 2, p. 361-364. San Juan.
- Ramos, V.A. 1985a. El Mesozoico de la Alta Cordillera de Mendoza: Facies y desarrollo estratigráfico, Argentina. In Congreso Geológico Chileno, No. 4, Actas, Vol. 1, p. 1-492-1-513. Antofagasta.
- Ramos, V.A., 1985b. El Mesozoico de la Alta Cordillera de Mendoza: reconstrucción tectónica de sus facies-Argentina. In Congreso Geológico Chileno, No. 4, Actas, Vol. 1, p. 2-104-2-118. Antofagasta.
- Reynolds, J.H.; Jordan, T.E.; Johnson, N.M.; Damanti, J.F.; Tabbutt, K.D. 1990. Neogene deformation of the flat-subduction segment of the Argentine-Chilean Andes: magnetostratigraphic constraints from Las Juntas, La Rioja Province, Argentina. Geological Society of America, Bulletin, Vol. 102, p. 1607-1622.
- Schiller, W. 1912. La Alta Cordillera de San Juan y Mendoza y parte de la Provincia de San Juan. Ministerio de Agricultura de la Nación, Sección Geología, Mineralogía y Minería, Anales, Vol. 7, No. 5, p. 1-68. Buenos Aires.
- Sclater, J.G.; Christie, P.A.F. 1980. Continental stretching: an explanation of the post-mid-Cretaceous subsidence of the central North Sea basin. *Journal Geophysical Research*, Vol. 85, p. 3711-3739.
- Sempere, T.; Marshall, L.G.; Rivano, S.; Godoy, E. 1994. Late Oligocene-Early Miocene compressional tectonosedimentary episode and associated land-mammal faunas in the Andes of central Chile and adjacent Argentina (32-37°S). *Tectonophysics*, Vol. 229, p. 251-264.
- Snyder, D.B. 1988. Foreland Crustal Geometries in the Andes of Argentina and the Zagros of Iran from Seismic Reflection and Gravity Data. Ph.D. Thesis (Unpublished), Cornell University, 196 p. New York.
- Valencio, D.A. 1980. El magnetismo de las rocas. Editorial Universitaria de Buenos Aires, 351 p.
- Vergara, M.; Charrier, R.; Munizaga, F.; Rivano, S.; Sepúlveda, P.; Thiele, R.; Drake, R. 1988. Miocene volcanism in the central Chilean Andes (31°30'S-34°35'S). Journal of South American Earth Sciences, Vol. 1, No. 2, p. 199-209.
- Vicente, J.C. 1972. Apercu sur l'organization et l'evolution des Andes argentino-chiliennes centrales au parallele de Aconcagua. International Geological Congress, No. 24, Section 3, p. 42-436. Canada.
- Windhausen, A. 1931. Geología Argentina. Geología Histórica y Regional del Territorio Argentino. *Jacobo Peuser Ltda.*, Vol. 2, 64 p. Buenos Aires.
- Yrigoyen, M.R. 1993. Los Depósitos Sinorogénicos Ter-

ciarios. In Relatorio, Geología y Recursos Naturales de Mendoza (Ramos, V.A.; editor), In Congreso Geológico Argentino, No. 12 y Congreso de Exploración de Hidrocarburos, No. 2, p. 123-148. Mendoza.

Yrigoyen, M.R. 1979. Cordillera Principal. In Simposio de Geología Regional Argentina, No. 2, Academia Nacional de Ciencias, Vol.1, p. 651-694. Córdoba. Zambrano, J.J. Mapa geológico de la provincia de San Juan y alrededores (Inédito), scale 1:500,000. INPRES, San Juan, Argentina.

Zambrano, J.J. Mapa geológico de la Provincia de Mendoza (Inédito), scale: 1:500,000. INPRES, San Juan, Argentina.

Manuscript received: April 25, 1996; accepted: June 7, 1996.